Research on Supersonic Combustion and Scramjet Combustors at ONERA

D. Scherrer, O. Dessornes, M. Ferrier, A. Vincent-Randonnier, Y. Moule, V. Sabel'Nikov

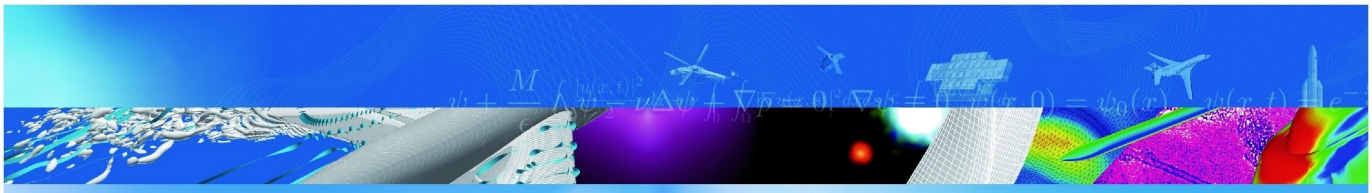

ARTICLE DE REVUE

Research on Supersonic Combustion and Scramjet Combustors at ONERA

D. Scherrer, O. Dessornes, M. Ferrier,
A. Vincent-Randonnier, Y. Moule, V. Sabelnikov

AEROSPACELAB JOURNAL

No 11, AL11-04, 20 pages

TP 2016-553

70 2016 ans

ONERA

THE FRENCH AEROSPACE LAB

D. Scherrer, O. Dessornes, M. Ferrier, A. Vincent-Randonnier, Y. Moule, V. Sabel'nikov
(ONERA)

E-mail: dominique.scherrer@onera.fr

DOI : 10.12762/2016.AL11-04

Research on Supersonic Combustion and Scramjet Combustors at ONERA

An overview of selected ONERA research activities on supersonic combustion and scramjet propulsion for civilian applications since 1992 is presented. The main part is devoted to basic research on supersonic combustion, including experimental database acquisition and combustion modeling. More applied studies on injection and flame stabilization in research scramjet combustors are then described and the article ends with a presentation of activities dedicated to real scramjet combustor design and characterization. This research was carried out either within the framework of three majors programs, PREPHA (1992-1997), JAPHAR (1997-2001), and LAPCAT II (2008-2013), or with internal funding.

Introduction

Supersonic combustion has been a research topic at ONERA since the 1960s. Supersonic combustion tests in simple configurations were performed between 1962 and 1967 at the Palaiseau research center [1]: this research demonstrated the possibility of achieving stable combustion with liquid kerosene and gaseous hydrogen in a Mach=2.5-3 air flow. At the same time, system studies concluded to the possibility of operating a fixed geometry dual mode ramjet for a flight range between Mach 3 and Mach 7 [2]. An important program, ESOPE, was then initiated in 1966 to assess the propulsive balance of an axisymmetric dual mode ramjet by means of ground tests and to compare it to the theory [3]. This activity was sustained by basic research on mixing and ignition in a supersonic air flow [4][5]. The ESOPE engine was tested under Mach 6 conditions in the ONERA Modane S4 hypersonic wind tunnel. Only transonic combustion was obtained under these flight conditions: the flow was choked somewhere in the combustor so combustion started in the subsonic regime and continued in the supersonic regime after the thermal throat. Tests under Mach 7 conditions, where supersonic combustion was expected, were finally not performed due to the cancellation of the program in 1972: it was then considered that hypersonic airbreathing propulsion was plagued with too many uncertainties, in particular in assessing the propulsive balance, and priority was given to rocket engines for high-speed propulsion.

The renewal of supersonic combustion studies at ONERA dates from 1992 with the PREPHA program (1992-1997), which involved ONERA and all of the French aerospace industry, under the aegis of the CNES, the DGA and the Research Ministry [6]. The main goal of the program was to study and ground-test the components (air intake, combustor, nozzle) of a scramjet concept for a space launcher application. In addition to the development of know-how for the design of scramjet components, this program provided the opportunity to develop high-enthalpy propulsion facilities at ONERA Palaiseau (Laerte for basic research on supersonic combustion and ATD5 for small scale scramjet combustors) and AEROSPATIALE Le Subdray for larger scramjet combustors. The large scale scramjet CHAMOIS was tested under Mach 6 conditions at AEROSPATIALE Le Subdray and the small scale scramjet MONOMAT was tested under conditions between Mach 4 and Mach 7.5 in the ATD5 facility at ONERA. In parallel, an important activity was dedicated to combustion modeling and validation, including the acquisition of an experimental database on supersonic combustion and the development of suitable optical diagnoses.

At the end of the PREPHA program, the DLR and ONERA decided to engage in a common research activity on airbreathing hypersonic propulsion: the JAPHAR program (1997-2001) [7][8]. The studies were anchored on a 10 m long experimental vehicle in the Mach 4 to 8 flight range. The experimental and numerical studies concerned all of the vehicle components, but the largest part of the activities was dedicated to the fixed-geometry dual-mode ramjet combustor. Tests of this combustor in the ATD5 facility demonstrated the capacity to operate the combustor in the various expected combustion regimes depending on the flight Mach number. In parallel, the experimental database initiated in the PREPHA program was completed with new measurements.

After the JAPHAR program, scramjet research at ONERA was reoriented mainly towards military applications, but a significant activity was maintained on civilian applications. In 2003, common experimental research on strut injectors for scramjet combustors was undertaken between ONERA and JAXA [9]. Between 2008 and 2013, ONERA participated in the LAPCAT II European program, aiming to develop technologies for a hypersonic passenger transport aircraft [10][11]. In parallel, a continuous combustion modeling and CFD code development activity was maintained with internal funding.

This paper gives an overview of the most significant research activities at ONERA since 1992 in the field of scramjets for civilian applications. They are presented from the most fundamental to the most applied. Following this introduction, the second part of the article is dedicated to the acquisition of an experimental database on supersonic combustion within the framework of PREPHA and JAPHAR programs. The third part deals with supersonic combustion modeling. In the fourth part, we present some studies on injection (ONERA-JAXA cooperation) and flame stabilization (LAPCAT II) in research scramjet combustors. Finally, the fifth part is dedicated to the design and study of scramjet combustors within the framework of JAPHAR and LAPCAT II programs.

Experimental database on supersonic combustion with axial and wall injection

Within the framework of PREPHA (1992-1997) and JAPHAR program (1997-2001), a quite complete experimental database on supersonic combustion has been set up at Onera on the Laerte combustor for the sake of code validation (Figure 1). This small size combustor (45×45 mm² in entrance) has a constant section for a 370 mm length, followed by a slightly diverging part (1.15° half angle) for a 500 mm length. It is fed with air at Mach 2. The test rig is equipped with a heat exchanger, that brings the air flow temperature up to 800 K, and with a hydrogen burner with oxygen replenishment that finally provides a maximum stagnation temperature of 1850 K for a total pressure of 7 bar. This provides a static temperature of 1100 K at the combustor entrance, which ensures self ignition of the fuel (gaseous hydrogen). For fuel injection, two configurations are available. The first one is an axial injection at Mach 2 of a cylindrical 6 mm diameter jet, located 33 mm downstream of the combustor entrance, in the center of the air flow. The second one is a Mach 2 wall injection (not represented), at a 45° angle with the air flow, located on the upper wall, 86 mm downstream of the combustor entrance. The fuel is gaseous hydrogen, which can be heated to a maximum temperature of 500 K by a heat exchanger.

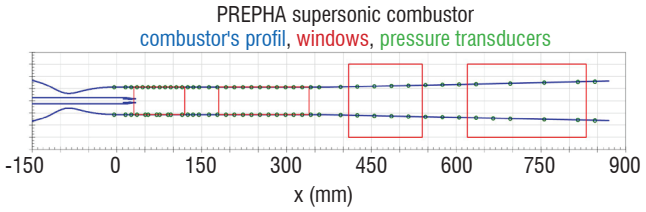

Figure 1- sketch of the Laerte combustor

For the axial injection, quite a complete database has been acquired on this configuration. It includes:

- wall pressure measurements;
- OH radical visualizations by spontaneous emission and PLIF [12], which also provides OH concentration (the calibration of the PLIF signal enables the mass fractions to be determined with an uncertainty of about 20%);
- H_2 jet visualizations by PLIF with acetone seeding [12];
- temperature measurements by CARS on N_2 and H_2 molecules [12][13];
- velocity measurements by laser interferometric velocimetry [14];
- velocity measurements by Particles Imaging Velocimetry (performed by a DLR Lampoldshausen team) [15];
- stagnation temperature measurements at the exit of the test channel.

For wall injection, the database includes:

- wall pressure measurements;
- OH radical visualizations by OH spontaneous emission and PLIF;
- H_2 jet visualizations by PLIF with acetone seeding;
- temperature measurements by CARS on H_2 molecules.

Figure 2 and Figure 3 show, for the axial injection at $x/D=30$ (D is the hydrogen jet diameter), the difference between OH visualization by spontaneous emission and by PLIF. For spontaneous emission, the signal is integrated over the entire width of the combustor and the exposure time is 1 ms, which averages the picture. Conversely, PLIF provides a view in the laser plane with a very short exposure time (12 ns), which allows the details of the reactive zone to be seen: it appears that combustion takes place at the periphery of the jet, in intermittent pockets.

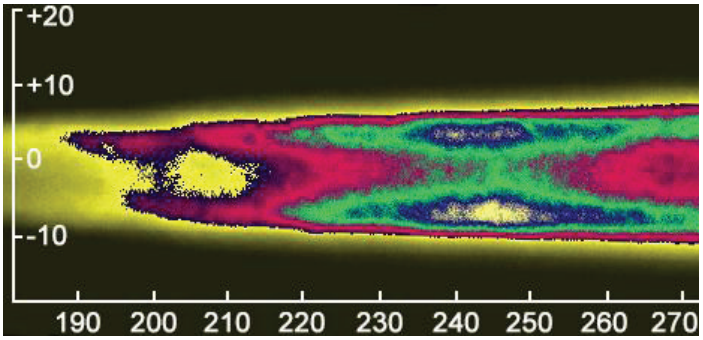

Figure 2 - Axial injection - OH spontaneous emission

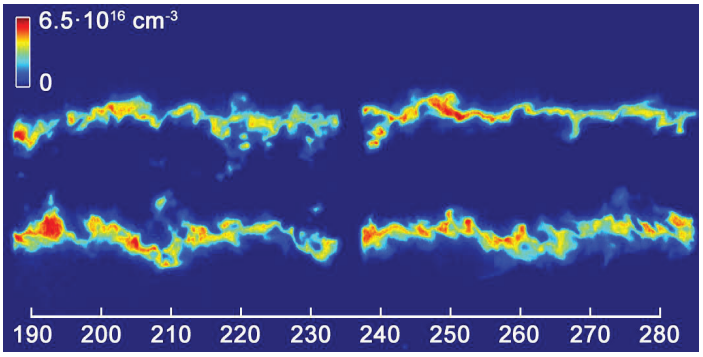

Figure 3 - Axial injection - OH visualization by PLIF

The collected data can be used for code validation. Figure 4 shows a comparison between the RANS computation and the experiment for the transverse contour of the OH mass fraction at $x/D=35$. Since the visualizations do not provide accurate absolute values, the experimental contour deduced from the PLIF visualization has been scaled, in order to fit the maximum value with the computed one.

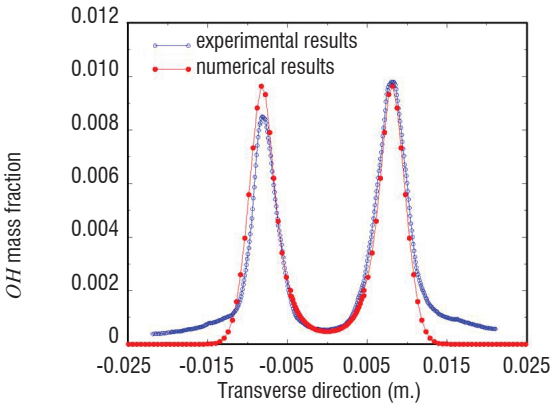

Figure 4 - Axial injection - OH mass fraction transverse contour

One can see that the position of the maxima is well respected by the computation, as well as the level inside the jet. A small discrepancy exists outside the jet, where the computed values vanish more quickly than the experimental ones.

Particle Image Velocimetry measurements were performed on the Laerte combustor for axial injection by a DLR Lampoldshausen team [15]. The application of PIV to high speed flows with large velocity gradients requires the use of submicron tracer particles, in order to minimize the particle slip velocity. In this case, the air flow was fed with Aerosil R812 particles (surface treated silica, hydrophobic, primary diameter 12 nm). Figure 5 provides an example of PIV measurement, slightly downstream from the injection, before ignition occurs. The measured velocity fields allow the instantaneous vortices to be visualized: they clearly show the structure of the flow and can be used, for example, to determine the size of the vortices and the shear layer expansion rate.

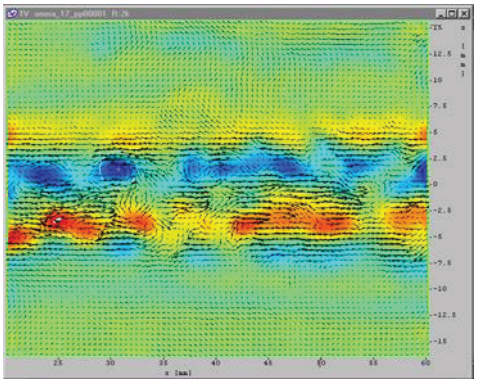

Figure 5 - Axial injection - PIV- Instantaneous velocity fluctuations (difference with mean values) and vortex strength

Instantaneous temperature measurements were obtained by Coherent Anti-Stokes Raman Scattering (CARS) on H_2 (inside the hydrogen jet) and N_2 (outside the jet) molecules. CARS thermometry is well suited for time-resolved measurements in turbulent flows. Figure 6 shows the transverse time-averaged temperature contour downstream from the injection, before ignition. The 160 K measured temperature in the jet core and the 1200 K temperature in the air flow are in agreement with the expected values.

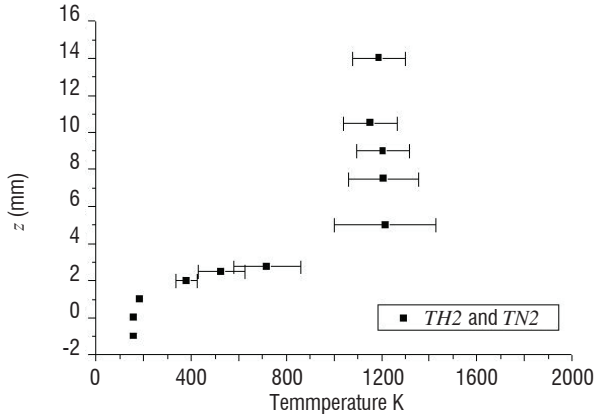

Figure 6 - Axial injection - CARS temperature measurement at x=43 mm (10 mm downstream from the injection)

Visualization of the hydrogen jet can be achieved by seeding the jet with acetone and performing PLIF on this molecule. This was done for wall injection in combination with PLIF on OH. These visualizations are illustrated in Figure 7. The exit from the wall injector (left) and a zone further downstream (right) were visualized. Pictures (a) and (c) correspond to PLIF on acetone and allow the hydrogen jet to be visualized. One observes that the jet remains adhered to the wall. Pictures (b) and (d) correspond to PLIF on OH. The residual OH due to the heater is visible, but one can see that no ignition exists in the vicinity of the injection: high OH signals are visible only in the second zone, firstly at the jet periphery, then quickly inside the jet, which indicates the presence of large-scale oscillations of the jet.

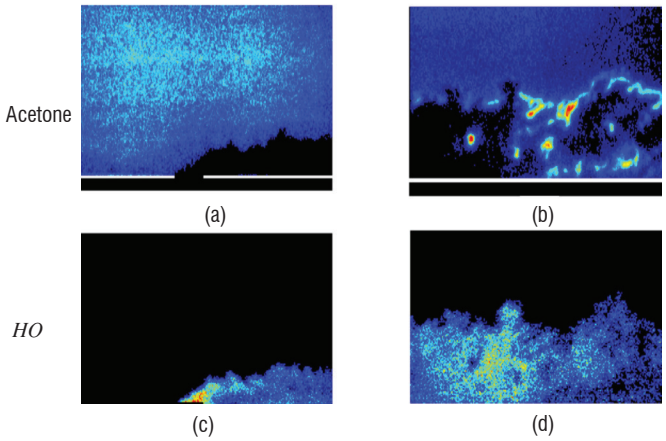

Figure 7 - Wall injection - Acetone and OH PLIF visualizations

Turbulent combustion modeling in supersonic flows

Due to the difficulty in reproducing true flight conditions in ground tests, computational fluid dynamics (CFD) offers an attractive tool for the study of high-speed turbulent reactive flows. However, the most standard closures for combustion modeling, which are based on the fast chemistry approximation, are not appropriate for such type of conditions, where combustion is largely governed by finite-rate chemistry effects and self-ignition phenomena.

Under these conditions, chemical reaction timescales indeed tend to have the same order of magnitude as turbulent timescales, with resulting Damköhler number values close to unity. In such combustion regimes, the application of fast chemistry assumptions associated with either equilibrium approximation or flamelet closures, where the flow field modeling is decoupled from chemistry, therefore becomes less appropriate, and finite-rate chemistry-based closures seem more appealing to describe supersonic combustion.

The focus of this study is thus on the development and validation of a finite-rate chemistry-based closure suitable for the description of supersonic combustion: the unsteady partially stirred reactor (U-PaSR) closure. The model is described in § "Turbulence-chemistry interaction (TCI) model: U-PaSR" and validation computations are presented in § "Validation of the model on the supersonic lifted jet flame of Cheng". Rather than the Laerte experiment, which has been extensively used in the past [16][17][18][19], the supersonic lifted jet flame of Cheng was retained for these validation computations, because this configuration presents the advantage of having been simulated by different teams, allowing fruitful comparisons.

Turbulence-chemistry interaction (TCI) model: U-PaSR

The high non-linearity of the instantaneous reaction rate $\dot{\omega}_k(T, Y_k)$ (Arrhenius Law) makes its filtered or averaged counterpart very difficult to model. When dealing with high-speed (supersonic)

combustion applications, a first-order simplification is often retained as a preliminary step, within the framework of the quasi-laminar (QL) combustion assumption, or homogeneous reactor (HR) approximation, which ignores the influence of the composition and temperature fluctuations: the subgrid scale (SGS) chemical rate of any k species is approximated by $\dot{\omega}_k\left(\tilde{T},\tilde{Y}_k\right)$, where $\tilde{\phi}$ designates the Favre average of a quantity ϕ. However, the composition and temperature fluctuations may play a crucial role in the thermal runaway processes that take place in the mixing layer until ignition occurs.

The unsteady partially stirred reactor (U-PaSR) model thus offers an interesting basis to incorporate the effects associated with these heterogeneities, within either a Reynolds-averaged Navier–Stokes (RANS) or a large eddy simulation (LES) framework. This model is an evolution of the Eddy Dissipation Concept (EDC) model introduced in the early works of Vulis [20], and Magnussen, see [21], [22], [23] .

Like the EDC model, the U-PaSR model relies on the highly intermittent character of turbulence and implies that chemical reactions are concentrated in fine-scale structures, where most of the viscous dissipation and molecular mixing processes take place. Turbulent mixing actually operates in the vicinity of very fine scale elongated structures, i.e., filament-like vortex structures or worms, the transverse dimension of which are of the order of the Kolmogorov length scale η_K (between 6 and 10 η_K). The structures that concentrate dissipation (mixing) processes coexist with non-homogeneous but weak vorticity zones, where scalar mixing is simply considered as inefficient for combustion. Following this physical representation of the flow, the U-PaSR model makes the assumption that each elementary volume of fluid is divided into fine-scale structure regions (denoted by *), featuring high scalar dissipation rate levels and surroundings (denoted by 0). The fine-scale structure regions (*) are supposed to behave like a perfectly stirred reactor (PSR), with potentially high reaction rates due to favorable mixing conditions. They are surrounded by other regions (0) featuring a vanishingly small reaction rate. From a mathematical point of view, the mean reaction rate $\bar{\dot{\omega}}_k$ can be expressed as:

$$\bar{\dot{\omega}}_k = \int_{\Psi} P(\psi)\dot{\omega}_k(\psi)d\psi$$

where P denotes the joint scalar PDF (Probability Density Function), $\psi=\left[T,Y_k\right]^T$ is the sample composition vector and Ψ is the associated domain of definition of the PDF. Considering the important levels of the mixing rate in zone (*), it is supposed to behave as a homogeneous medium and is thus represented in the PDF by a Dirac delta peak located at $\psi=\psi^*$. Strictly speaking, the zone (0) may be far from being homogeneous, since it is characterized by inefficient mixing levels but, for the sake of simplicity, the corresponding state (0) is also assimilated in the model to a single Dirac delta peak located at $\psi=\psi^0$: this approximation has no effect on $\bar{\dot{\omega}}_k$, since the reaction rates are vanishingly small in the zone (0). Thus, the resulting PDF is assumed to be bimodal:

$P(\psi)=\gamma^*\delta\left(\psi-\psi^*\right)+\left(1-\gamma^*\right)\delta\left(\psi-\psi^0\right)$, where γ^* denotes the volume fraction of the zone (*).

The mean chemical rate can then be expressed as:

$$\bar{\dot{\omega}}_k=\gamma^*\dot{\omega}_k\left(\psi^*\right)+\left(1-\gamma^*\right)\dot{\omega}_k\left(\psi^0\right)$$

Following the above discussion, the second contribution in this equation is considered to be zero. The mean chemical source term can therefore be rewritten as:

$$\bar{\dot{\omega}}_k=\gamma^*\dot{\omega}_k\left(\psi^*\right)$$

T^* and the Y_k^* are determined by the resolution of the following evolution equations:

$$\frac{\partial\bar{\rho}Y_k^*}{\partial t}+\bar{\rho}\frac{Y_k^*-Y_k^0}{\tau_m}=\dot{\omega}_k\left(T^*,Y_k^*\right)$$

$$\frac{\partial\bar{\rho}h^*}{\partial t}+\bar{\rho}\sum_{k=1}^{n}\frac{Y_k^*h_k^*-Y_k^0h_k^0}{\tau_m}=\sum_{k=1}^{n}h_{k_f}\dot{\omega}_k\left(T^*,Y_k^*\right)$$

These equations can be viewed as the mass and energy balance equations for the zone (*), where the convective terms have been neglected.

The state ψ^0 does not need evolution equations, since it can be determined by the relation $\tilde{\psi}$ ℵ$\gamma^*\psi^*$ $\left(1\quad\gamma^*\right)\psi^0$ where $\tilde{\psi}$ is provided by the gas solver. In practice, the only additional equations to be solved are the equations for h^* and Y_k^*, which can be rewritten as:

$$\frac{\partial\bar{\rho}\ddot{u}_{\ddot{u}}^*}{\partial t}+\bar{\rho}\frac{^*-\tilde{}}{\tau_m\left(1-\gamma^*\right)}=\dot{\omega}_k\left(T^*,Y_k^*\right)$$

$$\frac{\partial\bar{\rho}h^*}{\partial t}+\bar{\rho}\sum_{k=1}^{n}\frac{Y_k^*h_k^*-\tilde{Y}_k\tilde{h}_k}{\tau_m\left(1-\gamma^*\right)}=\sum_{k=1}^{n}\ddot{u}_{\ddot{u}_f}\,\dot{\omega}\left(\ ^*,\ ^*\right)$$

Finally, γ^* is modeled by the expression $\gamma^*=\tau_{ch}/\left(\tau_{ch}+\tau_m\right)$, where τ_{ch} is the chemical time scale and τ_m is the mixing time scale.

In this equation, τ_m is estimated as the harmonic mean value of the Kolmogorov time scale τ_k and the subgrid time scale τ_Δ, i.e., $\tau_m=\sqrt{\tau_K\tau_\Delta}$, where $\tau_\Delta=\Delta/\nu'$ and $\nu\ddot{u}=\sqrt{k/}$ (see [24], for instance). The Kolmogorov time scale is deduced from $\tau_K=\sqrt{\nu/\varepsilon}$, where $\varepsilon=k^{3/2}/\Delta$ and $k=\left(\frac{\nu_t}{0.069}\Delta\right)^2$.

There are different possible ways to estimate the chemical time scale τ_{ch} . Here, following a recent computational investigation performed with the same closure [25], it is evaluated by using the transit time obtained from a one-dimensional laminar premixed flame calculation performed at stoichiometry. The transit time is defined as the ratio of the premixed flame thickness δ_L to its propagation velocity S_L. The choice of this time to estimate the chemical time scale is retained only for the sake of simplicity. However, it seems worth noting here that, following the early analyses by Liñan, the characteristic chemical time scale that can be obtained from a diffusion flame at the limit of extinction is itself similar to the present estimate [26]. The choice of this peculiar time scale may therefore be relevant for both diffusion and premixed flames.

Validation of the model on the supersonic lifted jet flame of Cheng

Experimental setup and associated data

The NASA Langley Research Center (LaRC) has been deeply involved in the study of supersonic combustion over the years. Test campaigns were carried out on various experimental setups. Among these, a Mach 2 supersonic burner described by Jarret et al [27] was developed

and studied in detail by Cheng et al [28][29]. The purpose of such an experimental setup, schematically depicted in Figure 8, is to analyze the elementary physical processes involved in the auto-ignition of hydrogen-air mixtures and the stabilization of non-premixed combustion under supersonic conditions. From that perspective, sonic hydrogen is injected into a coflowing supersonic jet of hot vitiated air. The apparatus is axisymmetric and includes a cylindrical central fuel injector (2.36 mm in diameter) and an annular nozzle (17.78 mm in diameter). The vitiated air stream is accelerated through a convergent-divergent nozzle and reaches Mach 2 at a static temperature of 1250 K (see Table 1). Such a high value of the temperature favors the early development of the chemical processes within the mixing layer, leading to self-ignition and diffusion flame stabilization.

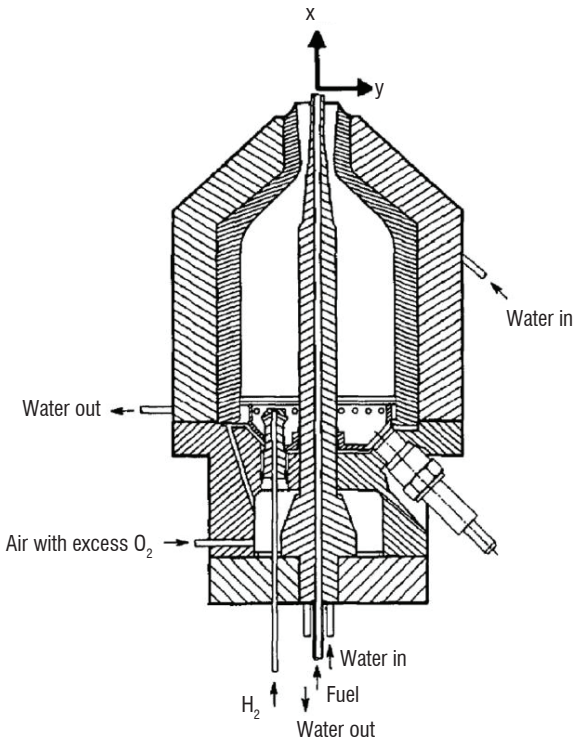

Figure 8 - Schematic diagram of the supersonic burner, from reference [29]

A primary combustion chamber provides the required stagnation conditions through hydrogen combustion in oxygen–enriched air. The combustion chamber and the fuel injector are water-cooled. However, even if the cooling water temperature is measured, its value is not reported in available references. The wall temperature profile in the combustion chamber therefore remains completely unknown. In addition to this, the internal geometry of the primary combustion chamber is not detailed. The nominal operating conditions studied by Cheng et al[29] are reported in Table 1.

Since both streams are slightly above ambient pressure at the nozzle exit, they give birth to a system of successive low amplitude compression and expansion waves. Multiple measurements were conducted in this geometry. Simultaneous measurements of temperature and species concentrations (main species and OH radical) were obtained by resorting to ultraviolet spontaneous vibrational Raman scattering and laser-induced predissociative fluorescence techniques. For instance, Jarett et al [27] reported mean temperature and chemical species (N_2 and O_2) concentration profiles resulting from coherent anti-Stokes Raman scattering measurements (CARS), as well as mean velocity profiles obtained by Laser Doppler Anemometry (LDA). The publications by Cheng et al [28] [29] gather mean and root mean square (RMS) profiles for temperature and mole fractions of major species O_2 , H_2 , H_2O , N_2 and OH at seven cross-sections located at axial distances $X/D = \{0.85; 10.8; 21.5; 32.3; 43.1; 64.7; 86.1\}$. Scatter plots of temperature and main species mole fractions are also available at six different locations $(X/D; Y/D) = \{(0.85, -0.65); (10.8, -0.65); (32.3, -1.1); (32.3, 1.1); (43.1, 0); (86.1, 0)\}$. The experimental database thus provides detailed data on the fluid mechanical scales and on the flow composition at $X/D = 0.85$, a very short distance from the nozzle exit compared to the experimental flame stabilization lift-off height ($X/D \approx 25$). Finally, Dancey [30] reported radial profiles of mean and RMS axial velocity measured with LDA. Experimental profiles of average data and associated RMS values have been gathered at seven distinct downstream locations for the major chemical species, namely, N_2 , O_2 , H_2 and H_2O, as well as for the OH radical and temperature. They have been evaluated from 500 to 2000 independent laser shots. The obtained RMS values reported by Cheng et al[29] confirm that temperature and species fluctuation levels can reach up to 20% and 40%, respectively. Given that the flame involves self-ignition, and combustion between non-premixed or partially premixed reactants under strongly fluctuating flow conditions, it offers a challenging test case for numerical simulation of high-speed turbulent combustion.

Geometrical parameters	
Nozzle exit i.d. (mm)	17.78
Fuel injector i.d. (D) (mm)	2.36
Fuel injector o.d. (mm)	3.81
Vitiated air conditions - Stagnation conditions	
Total pressure (Pa)	778,000 (±4%)
Total temperature (K)	1750
Vitiated air mass flow rate (kg/s)	0.09633 (±2.2%)
Exit conditions	
Pressure (Pa)	107,000
Temperature (K)	1250
Mach	2
Velocity (m/s)	1420
O_2 mode fraction (-)	0.201
N_2 mode fraction (-)	0.544
H_2O mode fraction (-)	0.255
Fuel conditions - Stagnation conditions	
H_2 ma&ss flow rate (kg/s)	0.000362(±3%)
Exit conditions	
Pressure (Pa)	112,000
Temperature (K)	545
Mach	1.0
Velocity (m/s)	1780
H_2 mode fraction (-)	1.0

Table 1- Supersonic burner nominal operation conditions

Large eddy simulation of the supersonic lifted jet flame

Numerical aspects

All computations were performed with the ONERA in-house code CEDRE, which is the reference tool at ONERA for energetics and multiphysics applications [32][33].

Computational domain and mesh

In order to properly specify the boundary conditions at the entrances, the internal geometry of the nozzle is included in the computational field. An important effort has been devoted to the representation of the nozzle exit and the description of the associated compressible shear layers. The computational field is supplemented by a large buffer region, to handle the far field boundary conditions without any numerical stability problems.

The mesh is composed of hexahedrons inside the flow field and prism layers alongside the walls. The characteristic cell size at the exit of the nozzle, inside the jet, is 0.2 mm. The prism layer alongside the walls of the primary combustion chamber is composed of five layers spread over a 0.1 mm thickness. Details of the mesh in the vicinity of the nozzle are represented in Figure 9. The number of cell elements of the final mesh is approximately 31,000,000. The whole mesh is divided into 480 domains handled by 480 bi-processor 3.07 GHz Westmere cores.

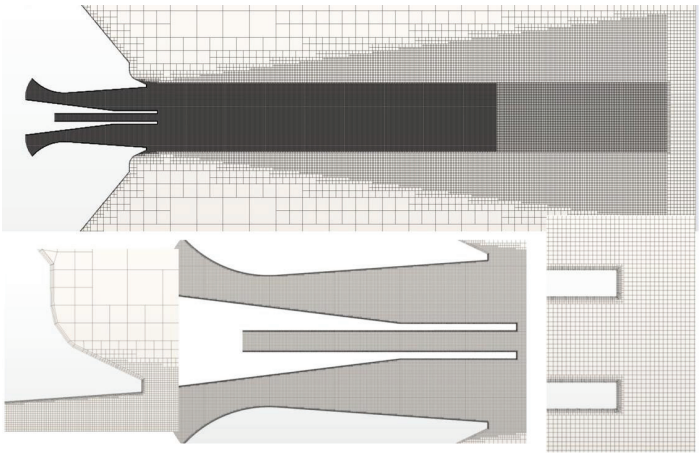

Figure 9 - Cheng lifted flame - Details of the mesh

Subgrid scale models

The subgrid scale turbulent viscosity μ_{SGS} is modeled through a standard Smagorinsky model, where the constant C_S has been set to 0.1. The U-PaSR closure is used to integrate the TCI effects. The chemical composition is described using nine species (H_2, H_2O, N_2, O_2, OH, H, O, HO_2 and H_2O_2) and the finite rate chemical reactions are described with the nineteen-step chemical scheme proposed by Jachimowski [31].

Numerical schemes

For this application, inviscid fluxes are computed using the HLLC (Harten-Lax-van Leer Contact) approximate Riemann solver proposed by Toro et al[34] and second-order accuracy is achieved via variable extrapolation, also often referred to as the Monotonic Upwind Scheme for Conservation Laws (MUSCL). It is applied in conjunction with Van Leer flux limiters to ensure the monotonicity of the numerical scheme. Temporal integration is processed with a second order explicit Runge–Kutta numerical scheme.

Boundary conditions

The boundary conditions at the entrances are set in terms of total quantities. A similar strategy has been retained in the RANS investigations conducted by Gerlinger [35] and Karl [36]. In practice, the stagnation temperature level of the vitiated air at the entrance has been set at 2050 K. This value, larger than that provided by Cheng in [29], enables the level of temperature to be recovered at the exit plane of the nozzle, which was measured by CARS and reported by Cheng [29]. Gerlinger [35] previously discussed the necessity of proceeding with such adjustments in his detailed investigation of the influence of inflow conditions on the numerical simulation of this lifted supersonic lifted flame. The experiments were carried out in a long-duration facility and therefore hot walls are considered to be isothermal at a temperature $T_w = 500$ K. No turbulence is injected at the entrances, mainly due to a lack of experimental data, especially for the turbulence spectrum, in the nozzle exit section.

Results and discussion

Flame structure

An instantaneous representation of the flame structure is depicted in Figure 10. In the top picture, a snapshot of the instantaneous temperature field superimposed with a H_2 mass fraction iso-surface (white) is provided. In the bottom picture, Q-criterion and OH mass fraction iso-surfaces are presented, both colored by temperature. Four regions can be outlined from the flame structure. The induction zone ($0 < X/D < 10$), the auto-ignition zone ($10 < X/D < 18$), the stabilization region ($18 < X/D < 26$), where the flame anchors at the beginning of a shock diamond and, finally, the end of the combustion zone ($30 < X/D < 34$).

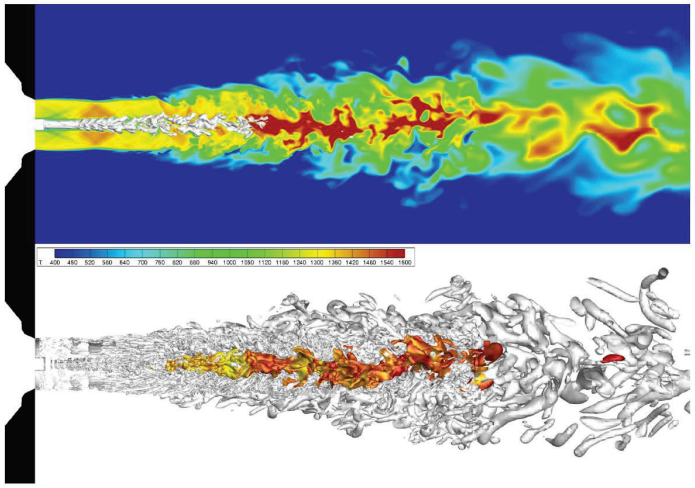

Figure 10 - Flame structure – Instantaneous field of temperature and H_2 mass fraction iso-surface [0.05] (top) - Iso-surfaces of Q-criterion [1x10^9 (s^2)] and OH mass fraction [0.01] colored by temperature (bottom)

The external mixing layer, between the ambient and vitiated air streams, develops quite differently from the internal mixing layer between the vitiated air and hydrogen coflowing jets. The value of the convective Mach number associated with the external mixing layer is so large that compressibility effects may play a quite important role.

This may restrict the mixing of ambient air with the vitiated air stream, since the growth and entrainment rates of compressible shear layers are known to be much smaller than those of incompressible flows at the same velocity and density ratios. This may also favor the birth of shocklet structures. Figure 10 shows that the transition from a two-dimensional destabilization mode to a fully developed three-dimensional mixing layer takes place rapidly. In comparison with the external mixing layer, the internal mixing layer that develops between the hydrogen jet and the vitiated air coflowing jet is characterized by a much smaller value of the convective Mach number, and therefore the two dimensional instability is the most rapidly amplified disturbance. From this figure, it can be noticed that the non-premixed jet flame is detached from the nozzle and it is found to stabilize at around twenty diameters from the injector exit plane, which is in satisfactory agreement with experimental results.

A typical instantaneous field of the heat release rate is reported in Figure 11. In practice, intensive heat release is located in regions that are micromixed at the present level of computational resolution, i.e., characteristic mesh size. At these locations, the fine-scale structure volume fraction γ^* is around unity, which confirms that these regions are chemically-controlled, see Figure 11. The auto-ignition region is characterized by an upstream peak in HO_2 radical formation in the middle of the jet. A detailed inspection of the flame stabilization region shows that it is significantly affected by a shock diamond structure positioned at $X/D \sim 20$, and this structure is itself significantly influenced by pressure waves issued from the external mixing layer. The compressible coflowing jet shock pattern indeed clearly contributes to the ignition of the hydrogen/air mixture inside the jet through shock-induced temperature rises.

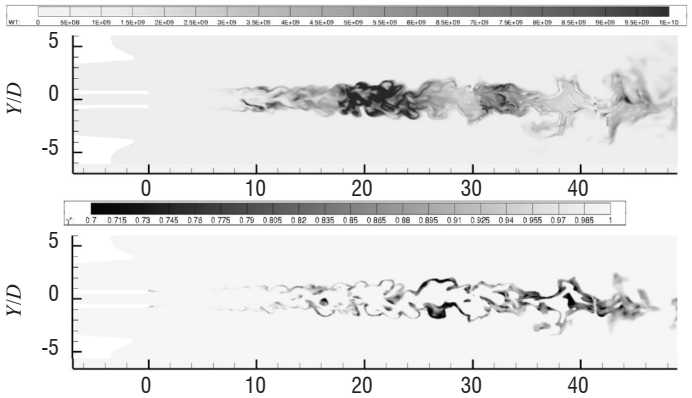

Figure 11 - Field of the instantaneous heat release (W m^{-3}) (top) - Instantaneous field of the volume fraction of fine-scale structures γ^* (bottom)

Temperature and composition profiles

We proceed here with a quantitative evaluation of our computational results. The mean and RMS profiles of the temperature and mole fractions of the main species are compared with experimental results on the symmetry axis, see Figure 12. It is noteworthy that the calculated RMS values are based on resolved temporal fluctuations only, i.e., without any consideration of the residual SGS fluctuations. The temperature rise along the flame axis calculated from the numerical simulation matches the experimental one quite closely. The mean lift-off height is predicted with a good level of accuracy; however, the flame temperature at the far end of the jet seems to be underestimated. The mean mole fraction profiles of hydrogen and water also seem to be quite well predicted. The mean oxygen mole fraction profile is the only one that displays some discrepancies with regard to the experimental results, especially in the far field. As observed in other numerical simulation results, see for instance [37], the oxygen mean concentration profile indeed exhibits a non-monotonic behavior, contrary to what is observed in the experiments. The first peak of the oxygen mole fraction (located at $X/D = 15$) is mainly due to mixing between the coflowing jets. The decrease afterwards is attributed to combustion in the stabilization region. Finally, the last increase of the oxygen mole fraction (starting from $X/D = 35$) is the outcome of an overestimated level of dilution with the external ambient air. The poor description of the external mixing layer development is the most probable reason that explains this incorrect representation of external air entrainment. The RMS profiles from the numerical simulation globally follow the experimental trend, except for hydrogen, for which the resolved fluctuations seem to be overestimated.

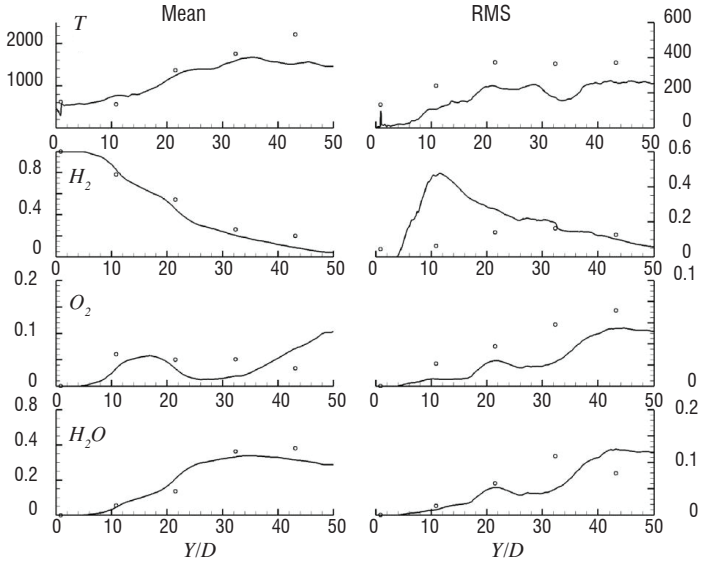

Figure 12 - Mean and RMS of the composition (temperature and mole fractions) on the symmetry axis - Comparison between numerical results and experimental data

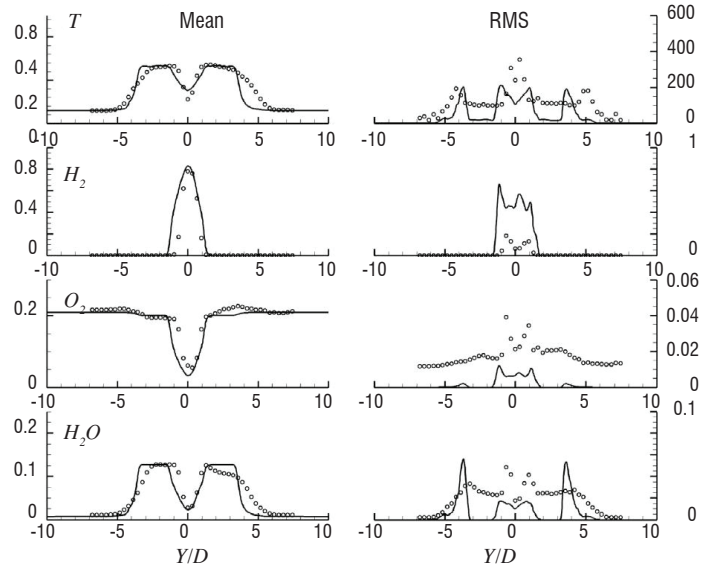

Figure 13 - Mean and RMS profiles of the temperature and main species mole fractions at $X/D = 10.8$

The mean and RMS profiles of the temperature and mole fractions of the main species are also compared with experimental results at four transverse sections (Figure 13 to Figure 16). The results from the numerical simulation of the mean quantities obtained in the first section ($X/D = 10.8$, Figure 13) compare well with the experimental results.

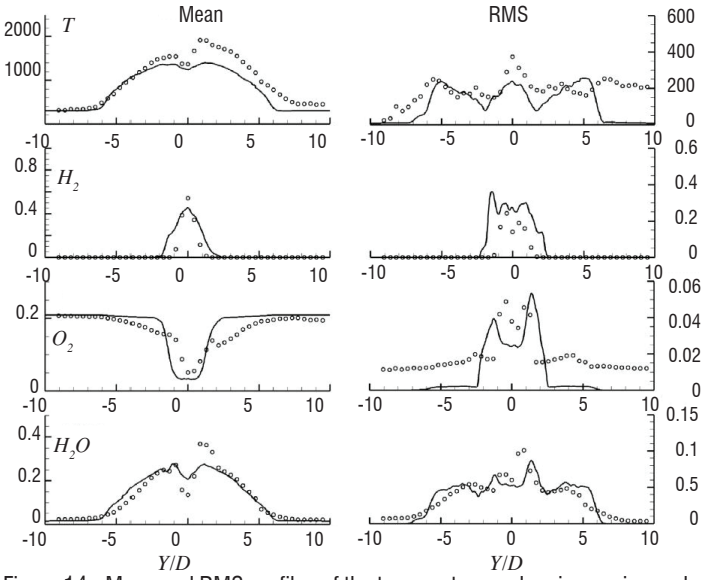

Figure 14 - Mean and RMS profiles of the temperature and main species mole fractions at $X/D = 21.5$

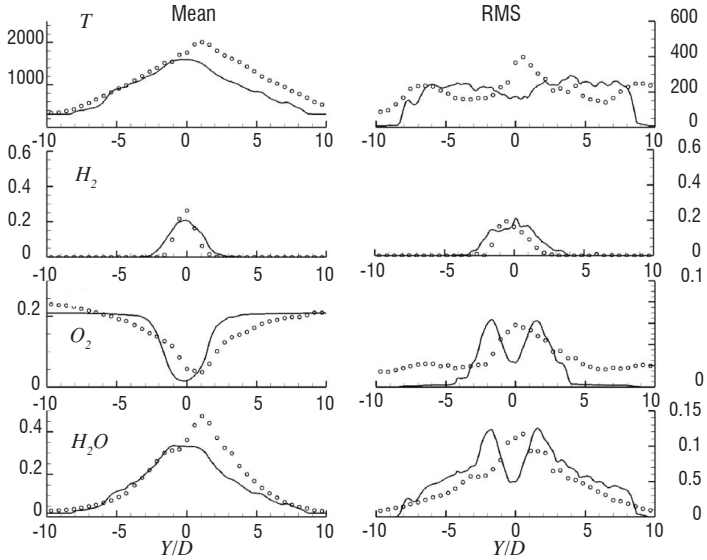

Figure 15 - Mean and RMS profiles of the temperature and main species mole fractions at $X/D = 32.3$

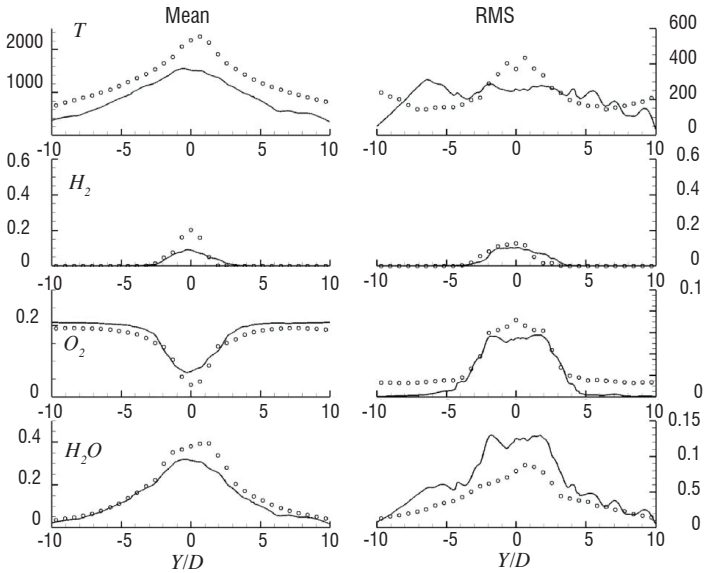

Figure 16 - Mean and RMS profiles of the temperature and main species mole fractions at X/D = 43.1

No particular asymmetry is observed. The outcoming flow seems to be well resolved, due to the combined use of a highly refined mesh at the exit of the nozzle and relevant boundary conditions settled in terms of total quantities. RMS trends and order of magnitude are correctly predicted, but the computed levels do not perfectly match the experimental measurements. The impact of standard steady boundary conditions is here clearly visible, especially on the RMS profiles of temperature fluctuations, the levels of which are significantly underestimated in the vitiated air stream. For these conditions, the description of the successive shock reflections (and expansions) off the boundary of the jet, and the resulting standing shock wave pattern in the jet (diamond structure or Mach structure) seems to be central to the quality of the numerical prediction, and temperature fluctuations appear to be of second-order importance to correctly predict the stabilization zone and lift-off height.

Except for the asymmetrical aspect, the numerical results again show a satisfactory agreement with the experimental data in the second section ($X/D = 21.5$, Figure 14). Hydrogen and oxygen profiles are especially well predicted. In this section, the prediction of composition fluctuations is also improved. The possible influence of unsteady boundary conditions seems to be unimportant at this location and the fluctuating quantities are much more impacted by the development of the two mixing layers, which seems to be well-captured. The RMS of temperature fluctuations is in satisfactory agreement with experimental measurements, except inside the hydrogen jet. However, it is worth noting that the mesh is not refined enough to satisfactorily describe the unsteady behavior of the external mixing layer and the associated ambient air entrainment. The levels of the oxygen concentration fluctuations are therefore greatly underestimated for $Y/D > 5$ or $Y/D < -5$.

In the following section ($X/D = 32.3$, Figure 15), the asymmetry of the experimental data still remains very marked. Mean profiles resulting from the numerical simulation match the lower branch of these asymmetrical data rather satisfactorily. The RMS profiles are in good general agreement with the results. The levels are relatively well predicted, except for the RMS of the temperature, as well as the RMS of the oxygen and water vapor concentrations inside the jet.

Finally, in the last section ($X/D = 43.1$, Figure 16), the whole mean temperature profile is underestimated by the numerical simulation, especially in the flame. However, RMS levels resulting from the numerical simulation are in good agreement with the experimental results for hydrogen and oxygen and, except inside the jet, they are also correctly represented for the temperature and water vapor concentration.

More detailed information on the U-PaSR model and associated validation computations can be found in [38] and [39].

Studies on injection and flame stabilization

Combustion of a transverse hydrogen wall jet in a supersonic air flow at very high flight Mach number

Designing a scramjet injection system is particularly challenging, since this device has to promote ignition, mixing and combustion while limiting total pressure losses. Sonic injection of fuel normal to the combustor wall is an interesting option for small size combustors. High temperatures are met in front of the jet because total temperature is recovered at this location, and pressure losses are moderate, since there is no injection strut. For these reasons, this flow configuration has been widely studied, mostly for non-reacting flows or for moderate supersonic Mach numbers [40][41][42][43].

run	P_{tot} (bar)	H_{tot} (MJ/kg)	M_∞	P_∞ (Pa)	T_∞ (K)	M^e	P^e (Pa)	T^e (K)	AoA (°)	PR
R1294	473	9.45	9.59	322	470	4.64	4545	1770	20	396
R1312	175	2.6	8.70	684	156	2.80	23391	990	30	214

Table 2 - Flow conditions

In this study, a Mach 1 hydrogen jet normal to a flat plate at angle of attack in a supersonic flow has been tested in the ONERA F4 hyper-enthalpy arc-heated wind-tunnel (see Figure 17).

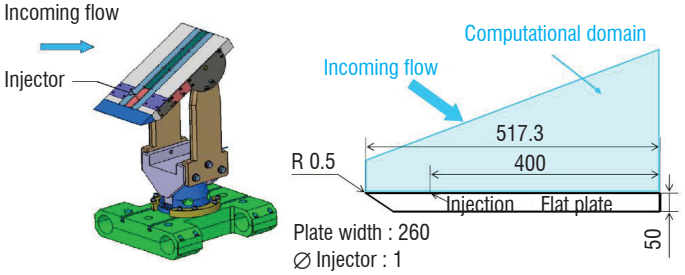

Figure 17 - CAD view of the plate - Sketch of the plate with computational domain

Two runs are considered here: R1294 and R1312. Table 2 gathers the flow conditions for these two runs: air total conditions (P_{tot}, H_{tot}), test section conditions (M_∞, P_∞, T_∞) and static conditions downstream from the leading edge shock, outside of the boundary layer (M^e, P^e, T^e). PR is the injection total pressure to static pressure ratio $PR = P_{tot,inj} / P^e$. The PR values are much greater than one, which indicates a highly under-expanded jet.

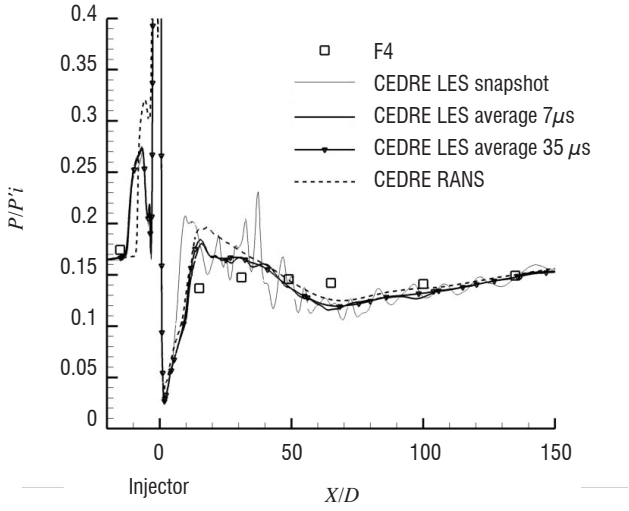

Figure 18 - R1294. Comparison between the experimental (F4) and computational (RANS and LES) pressure profiles on the symmetry plane.

LES (for R1294) and RANS (for R1312) simulations of this configuration have been performed using the ONERA code CEDRE. For R1294, experimental and numerical results are compared in Figure 18, in terms of pressure profiles in the symmetry plane. LES results are presented for a snapshot, a time integration over 7 μs, and over 35 μs. The comparison between the two integrated curves shows that a good time convergence has been reached (at least in terms of pressure distributions). A reasonable agreement is found between CFD and experiment, despite extreme flow conditions: high Mach numbers (9.59 in the far-field flow) and a large temperature range between the inside and near-field flow of the jet (see Figure 19).

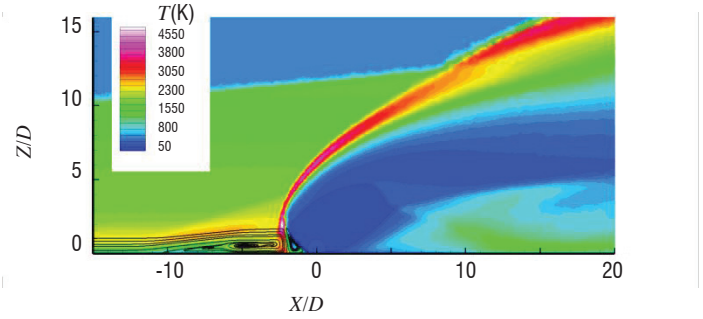

Figure 19 - R1294 (mean flow). Temperatures in the vicinity of the injection. Streamlines in the upstream boundary layer.

The dynamics of the flow are shown in the following animation (Figure 20), which presents the Mach number, a passive scalar and the OH mass fraction in the symmetry plane of the flow. The jet expands in the supersonic flow and then is recompressed by a barrel shock (see top view). This barrel shock generates an obstruction to the main flow, which reacts with a bow shock. Between these two shocks, a strong shear layer develops and creates large eddies that are responsible for turbulent mixing, as can be seen in the passive scalar plot. As soon as hydrogen is mixed with air in the shear layer, it immediately burns because of the high temperatures in this region. One can also notice high levels of OH mass fraction upstream from the injection, near the wall. This is due to the combustion of hydrogen that is trapped in the recirculation bubble, which forms because of the adverse pressure gradient encountered by the boundary layer flow as it approaches the bow shock foot (see also Figure 19).

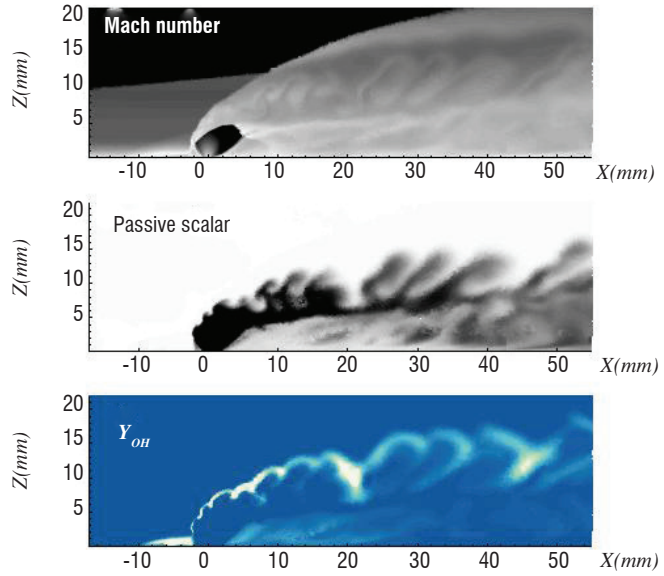

Figure 20 - Mach number animation (top), passive scalar (middle) and OH mass fraction (bottom) in the symmetry plane

Concerning Run R1312, the experimental OH^* visualization is compared, in Figure 21, to the calculated OH mass fractions (RANS) integrated over the width of the plate. For clarity reasons, the top view represents only the experimental results. A good agreement is observed between the experimental and numerical approaches.

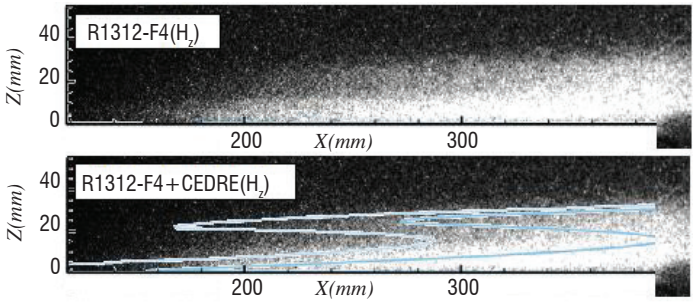

Figure 21 - R1312 - Experimental OH^* emission (top) and its comparison with computed mass fraction isolines (bottom)

Experimental characterization of strut injectors

Two major difficulties in supersonic combustion are the fuel-air mixing efficiency and flame stabilization. To overcome this, a variety of fuel injection schemes have been proposed and investigated extensively [44][45][46]. Strut injection is one of the candidates to enhance supersonic mixing, because it can introduce both fuel and vortices directly into the supersonic core flow. The technical difficulties in the application of strut injectors are the generation of vortices, ignition and flame stabilization. Streamwise vortices have been investigated extensively by trying various ways of generation and use [47][48][49][50]. The results revealed that, depending on how the streamwise vortices are generated and used, they can provide a significant mixing enhancement. The counterpart is an increase in the combustion pressure gradients, which can lead to separated regions and engine unstart. At ONERA and JAXA, strut injectors have been implemented in scramjet combustors and extensively tested. ONERA developed a multi-staged fuel injection strut, specifically designed to enhance ignition and flameholding near the strut base [45]. On the other hand, JAXA studied the use of streamwise vortices generated by "Alternating-Wedge struts" to enhance supersonic mixing and combustion [51][52][53]. In order to better understand the mixing and combustion mechanisms involved in both strategies, a joint program was set up in 2002 between ONERA and JAXA. The goal was to test different strut injector concepts in the same combustor and the same facility and to compare their performances in terms of mixing, ignition and combustion.

Test facility and combustor

Experiments were conducted in the supersonic combustion test facility implemented at ONERA/Laerte. The combustor was designed and manufactured by JAXA. It is connected to the test rig by a Mach 2.5 contoured nozzle (Figure 22). The combustor is fed with vitiated air, heated to 1620 K by two successive hydrogen burners. Oxygen is injected upstream from the auxiliary burners, in order to maintain the mole fraction of oxygen in the vitiated air flow at 21%. The facility air pressure storage is 25 MPa. Fuel is gaseous hydrogen.

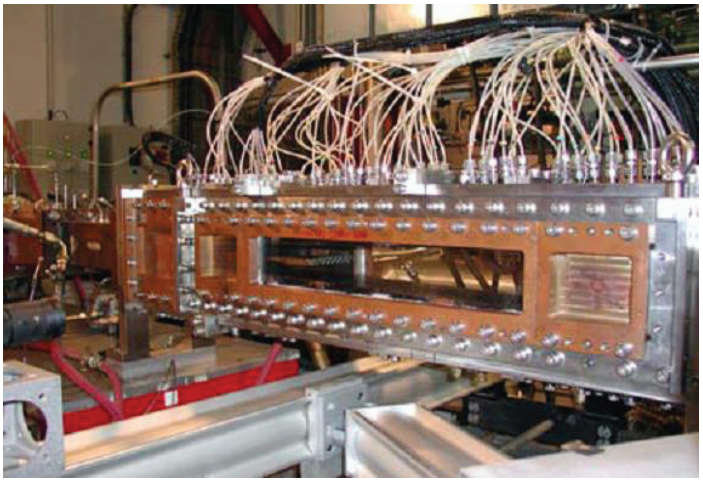

Figure 22 - View of the JAXA supersonic combustor connected to the Mach 2.5 nozzle

The combustor is basically two dimensional and has a 355 mm long constant area first part (50 mm × 100 mm cross section), followed by a 600 mm long diverging second part (expansion half-angle of 1.72° applied to top and bottom walls). The combustor has a constant 100 mm width. The whole combustor is made of copper. The tested strut injector is installed at the transition between the constant area section and the diverging section (Figure 23).

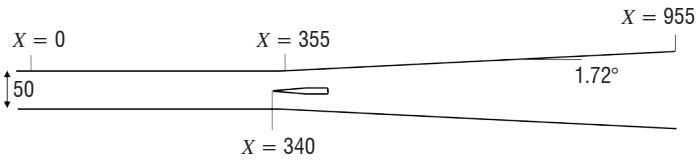

Figure 23 - Sketch of the JAXA supersonic combustor

The strut leading edge is located at x= 340 mm. Here, x is the longitudinal distance from the combustor entrance (i.e., the exit of the Mach 2.5 nozzle). For all of the struts, the fuel injection orifice is located at x = 433 mm.

Figure 24 - View of a strut injector in the combustor

Strut injector concepts tested

Five strut injector concepts were tested. They are shown in Figure 25 (ONERA concept, without streamwise vortices) and in Figure 26

(JAXA concepts, with streamwise vortices). The ONERA strut is made of a leading wedge followed by a constant section part. Fuel is injected at two levels: the first one at the walls of the strut (four jets on each side, directed at an angle of 45° with the walls), at the beginning of the constant section part, and the second one at the base of the strut (three jets parallel to the air flow). It will be named the "staged injection strut" in the following. The JAXA struts have a unique injection level, parallel to the air flow, and are characterized by alternating upward and downward expansion ramps arranged at the base of the strut in order to generate either counter-rotating or co-rotating streamwise vortices in the air flow: these vortices are at the origin of the mixing enhancement. Hydrogen is injected through 6 holes, each one directly on the axis of a streamwise vortex. The JAXA struts will be named "alternating wedge struts". A more detailed description of all of these injectors can be found in [54].

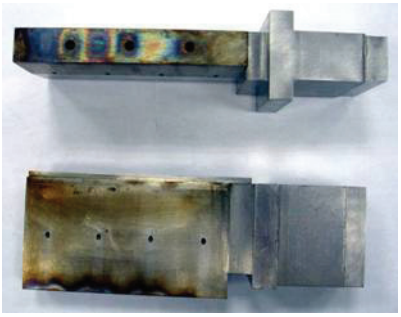

Figure 25 - ONERA strut injector concept (without streamwise vortices)

Figure 26 - JAXA strut injector concepts (with streamwise vortices)

Main results

The various injector concepts tested were compared through wall pressure measurements, spontaneous emission visualizations and OH-PLIF visualizations. We present here some results obtained with the staged injection strut named ONH10 in [54] and with the alternating wedge strut named CNR11-R36 in [54].

Spontaneous emission visualizations are presented in Figure 27. With the staged injection strut, stable ignition clearly takes place at the strut base, which acts as a flameholder. One observes that the lateral jets do not ignite spontaneously and seem to be ignited downstream, by the flame issued from the base jets: at this stage, the flame height increases suddenly and continues to grow more slowly downstream. The consequence is that combustion presents two regions: a first one, very stable but rather thin, which concerns only the base jets, and a second one, much larger, when the combustion has propagated to the lateral jets. On the other hand, ignition seems somewhat less stable with the alternating wedge strut, but it apparently occurs for all jets at a short distance from the strut base. Then, the flame height increases rapidly due to the effect of the streamwise vortices.

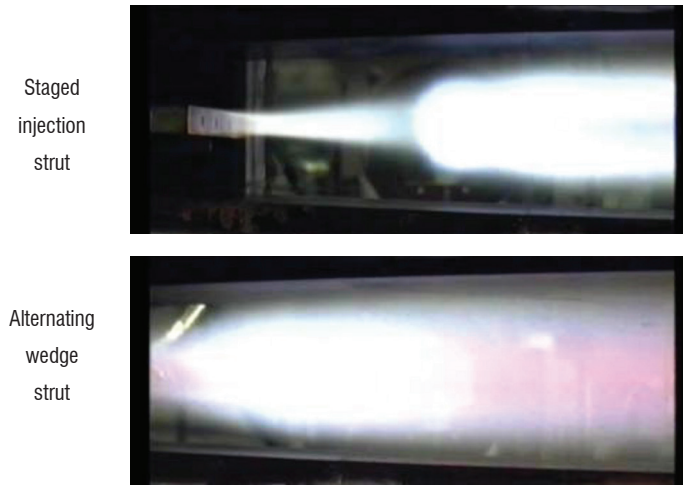

Figure 27 - Spontaneous emission visualization for the staged injection strut (top) and the alternating wedge strut (bottom)

The instantaneous OH-PLIF images in two transverse planes (x=40 mm and x=100 mm from the strut base) confirm this tendency (Figure 28). It is clearly visible that the alternating wedge strut actually generates larger scale motion in the combustor cross-section compared to the staged injection strut. However, the ignition is less stable and does not concern the central jets in a first step; this was not visible from the spontaneous emission images, which integrate the emission over the whole width.

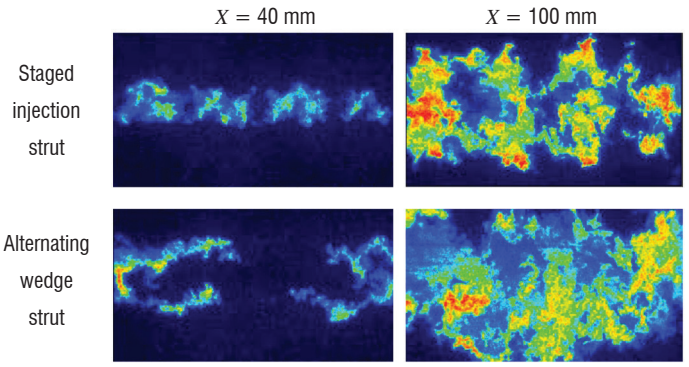

Figure 28 - Instantaneous OH-PLIF images at x=40 mm (left) and x=100 mm (right) for the staged injection strut (top) and the alternating wedge strut (bottom)

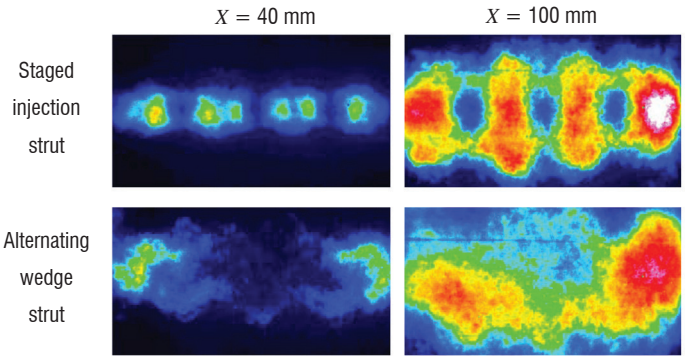

Figure 29 - Time-averaged OH-PLIF images at x=40 mm (left) and x=100 mm (right) for the staged injection strut (top) and the alternating wedge strut (bottom)

The better efficiency of the alternating wedge strut seems a little less obvious when one looks at time-averaged OH-PLIF images (Figure 29): combustion is actually more spread out with the alternating wedge strut, but not necessarily much more efficient.

These tendencies are confirmed by the wall pressure rise (not represented here), higher all along the combustor for the alternating wedge strut, except at the end, where the pressure is similar for all struts (see [54]) indicating that the global combustion efficiency may be not so different. More detailed information on these results can be found in [54].

It should be added that, more recently, numerical simulations of this combustor were performed by C. Fureby [55]. The computational results provide precious help in understanding the experimental results.

Experimental study of self-ignition and combustion in a research scramjet

Since 2010, the Laerte facility at ONERA – Palaiseau has been equipped with a new dual-mode ramjet combustor (Figure 30), which was developed, manufactured and used within the LAPCAT II project (EU 7th Framework Program, 2008-2013 [56][10][11][57]). The goal of the study was to investigate the self-ignition conditions in the combustor, in order to evaluate the effect of air vitiation on ignition. The internal geometry of the combustor was identical to that initially developed by ITLR, which was in charge of pure air tests.

The combustor (Figure 31) comprises four parts: the first (55 mm < x_1 < 280 mm) has a constant cross-section, the following sections (280 mm < x_2 < 598 mm < x_3 < 952 mm < x_4 < 1257 mm) have, respectively, diverging half-angles of 1°, 3° and 1° to prevent/stunt thermal choking. Large fused silica windows can be placed at different locations, allowing optical access. The combustor is fed with hot vitiated-air (heating by H_2/air combustion and O_2 replenishment to maintain the O_2 molar fraction at 0.21). The total temperature and pressure can reach up to 1800-1900 K and 1.0-1.2 Mpa, respectively. The supersonic flow is generated by a De Laval nozzle (Mach = 2.0 in this case, Mach = 2.5 being also available). The facility is operated in the blow-down mode, with the mock-up walls working as a heat-sink. The combustion chamber is made of a copper alloy and the inner walls include a 0.3 mm thick YSZ (Yttria-Stabilized Zirconia) thermal barrier coating. The combustor outlet is connected to a 400 mm diameter exhaust pipe, where the pressure is around 0.1 MPa. A computer controls the reproducibility and stability of the operating conditions.

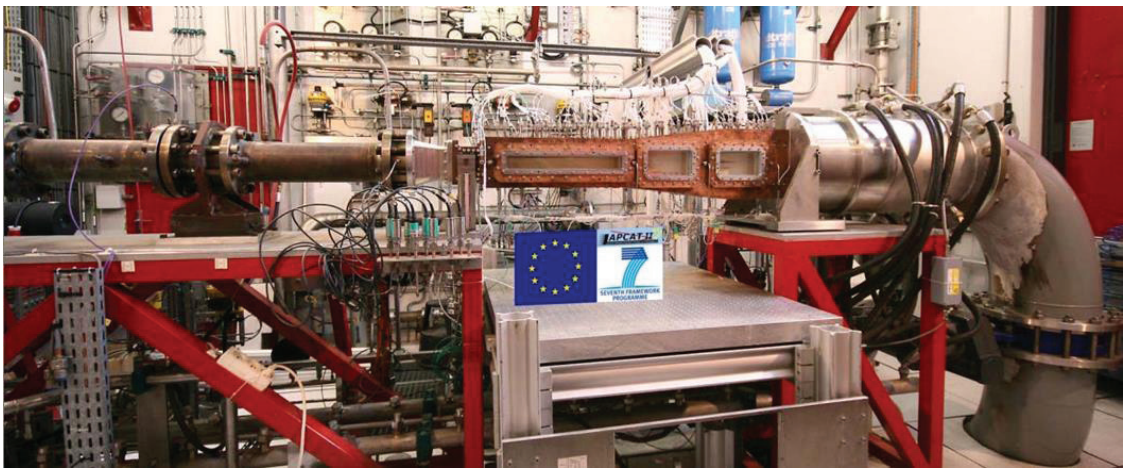

Figure 30 - Lapcat2 combustor installed in the Laerte facility

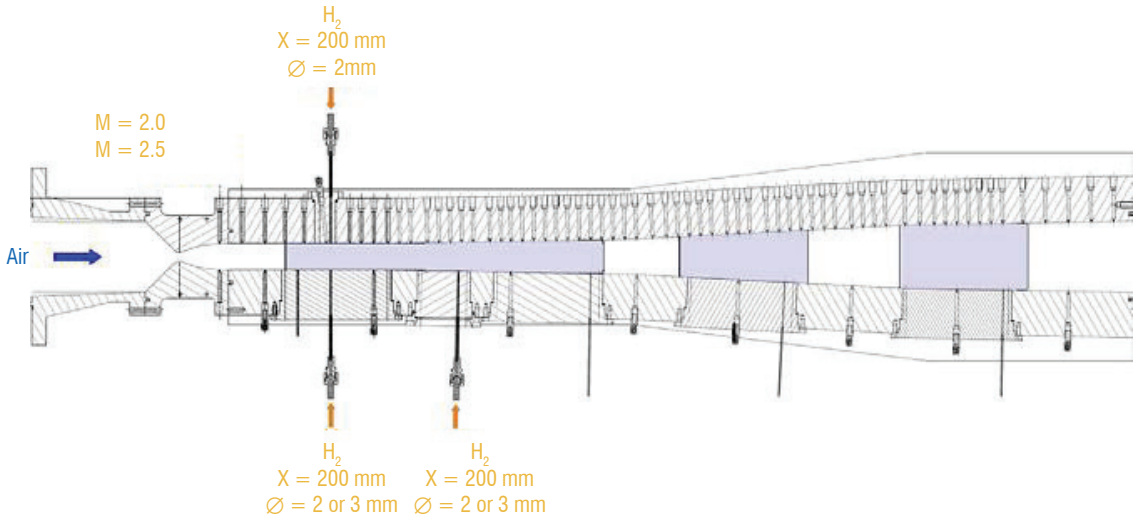

Figure 31 - Side view of the combustor equipped with wall hydrogen injectors

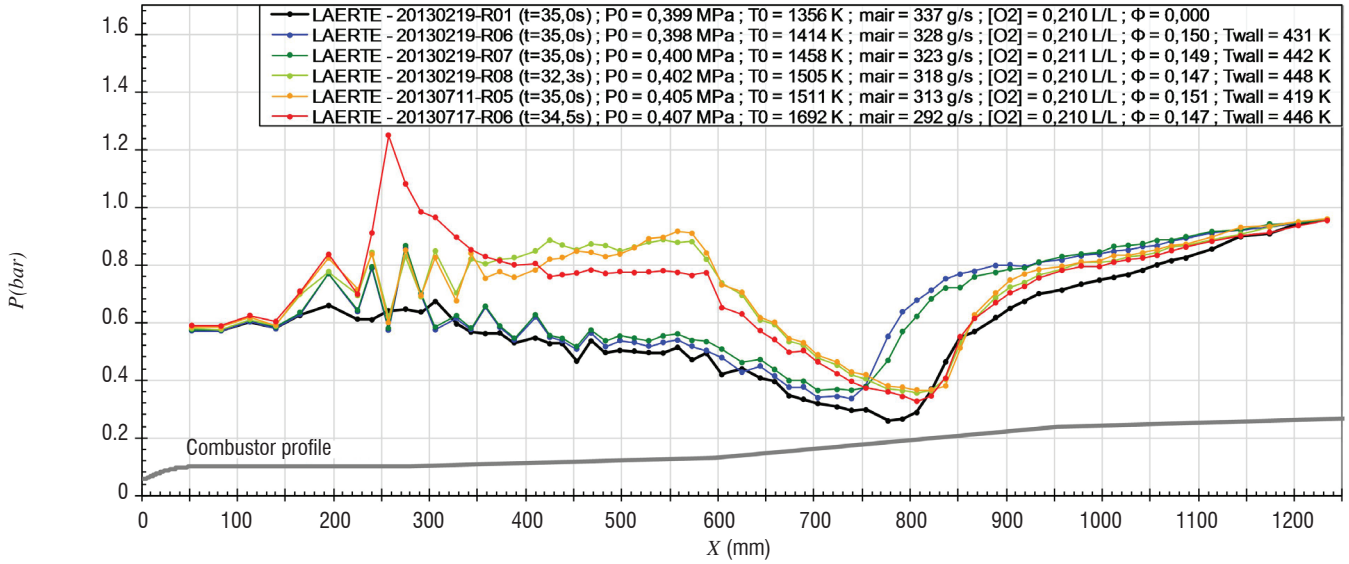

Figure 32 - Pressure profiles for increasing T_0 (P_0 = 0.40 MPa and $E.R.$ = 0.15)

The fuel used was pure gaseous hydrogen. Injection can be achieved from single sonic injectors located in the upper and lower walls, at x = 200 mm (upper wall, lower wall, or both) or at x = 368 mm (lower wall only). For the tests presented here, we used the two ϕ=2 mm injectors at x = 200 mm.

Given that the combustor is not water cooled, the overall duration of a test run is limited to around 1 minute, but the useful duration, i.e., at the required temperature, lasts between 5 s and 15 s, depending on the test conditions.

The ignition limit for the supersonic combustion of wall injected hydrogen in a hot air cross-flow has been explored with tests at various total temperatures, for the same equivalence ratio ($E.R.$ = 0.15). The wall pressure profiles are presented in Figure 32. Without injection, the pressure profile indicates a supersonic expansion in the diverging parts of the combustor, up to the separation of the flow at $x\approx$ 800 mm due to overexpansion. With injection, three regimes can be identified from the pressure profiles, depending on the total temperature.

For T_0 = 1414 K and T_0 = 1458 K, no significant supersonic combustion can be observed: combustion occurs only downstream from the separation shock. The injection shock and its successive reflections are visible from x = 200 mm.

For T_0 = 1505 K and T_0 = 1511 K, the static temperature is sufficient to allow self-ignition of hydrogen at $x \approx$ 310 mm, just after the beginning of the first diverging section. Ignition is followed downstream by a weak supersonic combustion. The pressure profiles for these two temperatures are nearly identical.

For T_0 = 1692 K, ignition occurs closer to the injection, at $x \approx$ 240 mm, and is at the origin of a flow separation, which results in a high pressure peak.

These results are confirmed by the flow visualizations presented in Figure 33 for three values of T_0. For T_0 = 1414 K (Test Run 20130219-R06), combustion is visible only in the second window: around 659 mm ≤ x ≤ 828 mm). For T_0 = 1458 K (Run 20130219-R07), combustion mostly occurs in the same region, but a faint emission seems to be visible along the last third of the first window and a small pressure increase is noticed in the pressure profile (Figure 32). This could perhaps correspond to a cool flame. For T_0 = 1505 K (Run 20130219-R08), supersonic combustion is clearly visible through the first window, with ignition at $x \approx$ 310 mm.

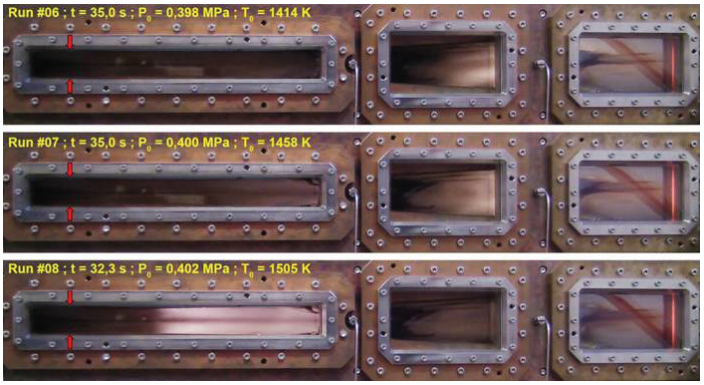

Figure 33 - Images of the combustion for increasing T_0 (P_0=0.40 MPa and $E.R.$=0.15) ; red arrows indicate the position of the fuel injection

Schlieren imaging technique (Figure 34) gives complementary information on the fuel injection, mixing and ignition processes (P_0 = 0.41 MPa, T_0 = 1697 K, $E.R.$ = 0.15). An injection pattern consisting in a bow-shock and barrel shock is clearly visible (around x = 195–205 mm), as described in the literature [58]. Downstream from the fuel injection point, the mixing region is evidenced. 50 mm to 80 mm downstream from the injection point, a kind of λ-shock system oscillates, in the wake of which combustion starts. The pressure peaks caused by the injection shocks and the λ-shock appear on the pressure profile at x = 200 mm and x = 240–260 mm, respectively (see also Figure 32 – 20130717-R06).

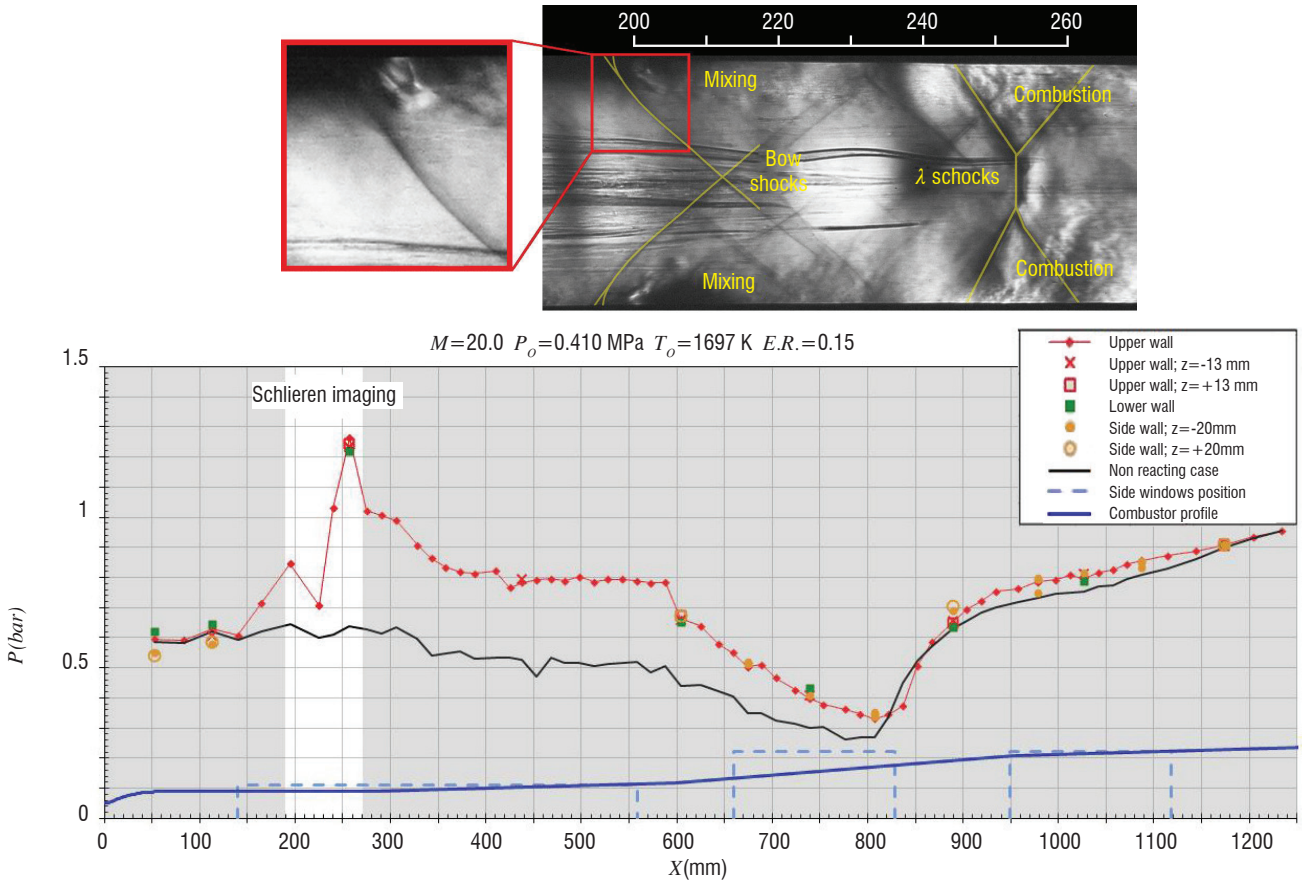

Figure 34 - Fuel injection and ignition (P_0 = 0.410 MPa, T_0 = 1697 K, $E.R.$ = 0.15)
Upper right: annotated Schlieren view (1280×504 pixels; 12 kHz)
Upper left: zoom on the injection region (128×128 pixels; 210 kHz)
Bottom: related pressure profile

This experimental study has been supplemented with a RANS numerical simulation of the supersonic combustion, revealing the prime effect of the wall conditions (temperature and roughness) on the ignition distance. Moreover, the ignition distance has been demonstrated to be significantly shorter in vitiated air than in pure air. More detailed information on both experimental and numerical aspects can be found in [56].

Design and study of scramjet combustors

Design, test and simulation of the JAPHAR dual-mode ramjet

In 1997, ONERA and the DLR decided to join their efforts on hypersonic air-breathing vehicles within the framework of the JAPHAR program. For this purpose, a vehicle demonstrator in the flight range Mach = 4 to 8 was chosen as a guideline for the studies, and a dual-mode ramjet engine was designed for this vehicle. In order to work as a dual-mode ramjet, the hydrogen fueled combustion chamber has two parts and two injection stages. The first part is slightly diverging and is mainly dedicated to supersonic combustion at a high flight Mach number, whereas the second one allows subsonic combustion at a lower flight Mach number, with a thermal throat located near the chamber end (Figure 35). The vehicle engine was defined to be completely supersonic at Mach 8 when all of the hydrogen is injected from the first injection stage. The length is roughly 2.4 meters.

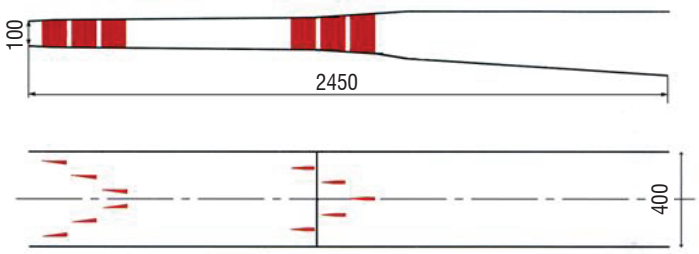

Figure 35 - Sketch of the Japhar vehicle dual-mode ramjet

The fuel injection distribution between the two injection stages enables the combustion regions to be controlled, as well as the position of the normal shock and of the thermal throat for the subsonic combustion regime.

Taking into account the capacities of the ONERA test facility, an experimental engine with smaller dimensions was extrapolated from the vehicle engine studied during the JAPHAR project (Figure 36). The chamber entrance cross-section is 100×100 mm² (100×400 mm² for one vehicle engine module). The chamber height and length are kept identical, but the injection system is modified to be suited to a smaller width. As a result, the first injection stage has only one strut and wall injections, whereas the vehicle chamber has several struts. The wall injectors of the experimental chamber enable a mixing representative of that achieved in the real chamber. The second injection stage is constituted by two struts.

In addition, to facilitate the strut assembly and to be able to modify the chamber geometry easily, the struts are oriented at 90° compared to the vehicle initial position (Figure 36 compared to Figure 35).

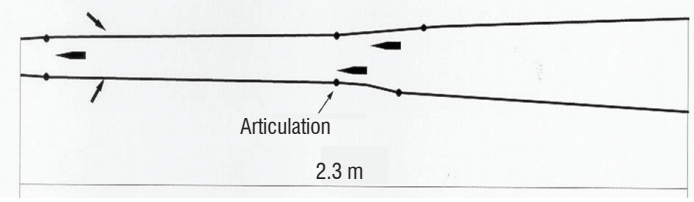

Figure 36 - Sketch of the JAPHAR experimental dual-mode ramjet

Figure 37 - View of the test setup in the ATD 5 test cell

Prior to the tests, the chamber was studied numerically using the ONERA in-house 3D reactive code CEDRE.

The computations predicted that this engine should allow three different combustion regimes to be obtained - subsonic, transonic and supersonic - depending on the flight Mach number, which is illustrated in Figure 38 where subsonic zones (blue regions) are shown and Figure 39, which represents the pressure fields for 3 different flight Mach numbers. In order to obtain these combustion regimes, the fuel injection distribution between the first and the second stage was 25% - 75% for Mach 5.3 and 6.6, 80% - 20% for Mach 7.5 .

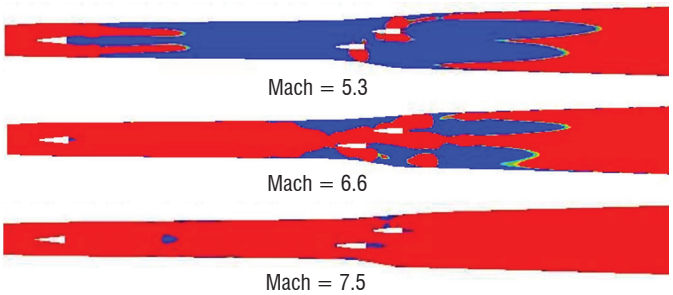

Figure 38 - Predictive computations - Sub/supersonic regions

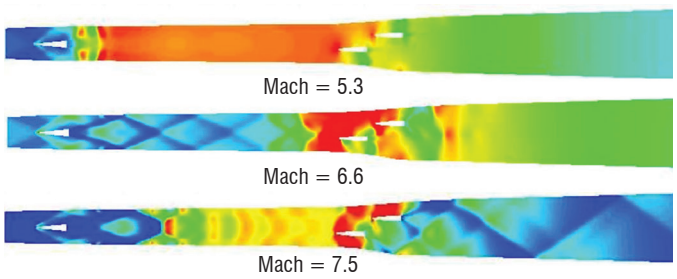

Figure 39 - Predictive computations - Pressure field

Tests campaigns were performed later for simulated flight Mach numbers of 4.9, 5.8 and 7.6. These values differ slightly from those retained for predictive computations, due to subsequent changes in the shape of the vehicle forebody. The actual test conditions are given in Table 3. New computations were performed after the tests with these conditions for test/computation comparisons.

M_∞	M_1	Pi_1 (bar)	Ti_1 (K)	P_1 (Pa)	T_1 (K)
7.6	3.11	29.0	2470	51450	1135
5.8	2.58	12.7	1500	59750	740
4.9	1.987	6.45	1171	81400	710

Table 3 - Test conditions

The air that was pre-heated through H_2 combustion and reoxygenation has the following mass fraction compositions (Table 4):

M_∞	O_2	N_2	H_2O
7.6	0.280	0.414	0.306
5.8	0.249	0.598	0.153
4.9	0.251	0.647	0.102

Table 4 - Inflow gas composition (mass fraction)

In addition to ER (Equivalence Ratio) exploration, several injection distributions were investigated throughout the tests (see Table 5).

Test case	1st level of injection	2nd level of injection
IR1	0%	100%
IR2	20%	80%
IR3	40%	60%
IR4	100%	0%

Table 5 - Tested injection distribution

For Mach 4.9 conditions, tests were performed with the IR1 and IR2 injection distributions. Figure 40 shows the fairly good agreement between test and computation at $ER=1$, with Injection Distribution IR2. The combustion regime is fully subsonic, with the normal shock located at the first injection strut and the thermal throat located just downstream from the second injection stage.

For Mach 5.8 conditions, the IR1, IR2 and IR3 injection distributions were experimented. The computed and experimental pressure distribution at $ER=1$ with Injection Distribution IR3 are shown in Figure 41. The combustion regime is partly subsonic and partly supersonic. The shock is located downstream from the first injection stage and the thermal throat is located at the second injection stage so that the fuel injected at this stage burns in a supersonic flow. The agreement between test and computation is again very good.

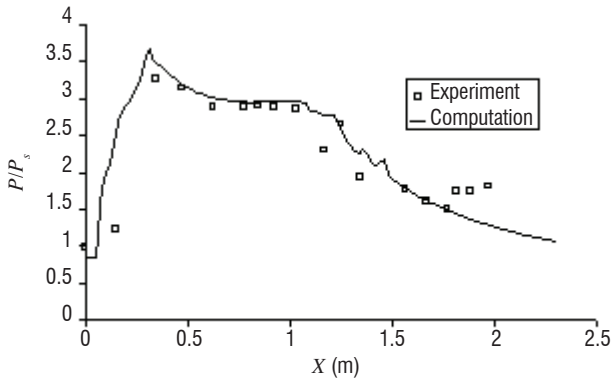

Figure 40 - Mach 4.9 - ER=1 - IR2 - Computed and experimental pressure distributions

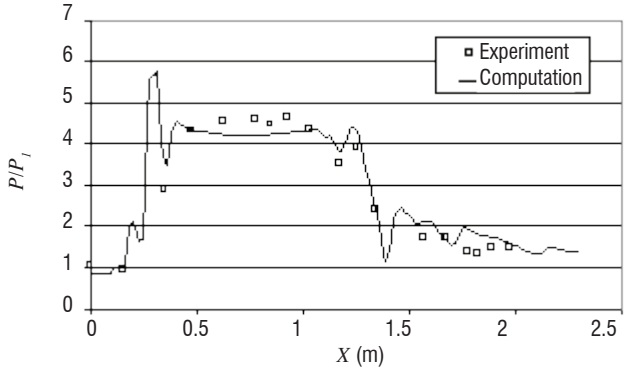

Figure 41 - Mach 5.8 - ER=1 - IR3 - Computed and experimental pressure distribution

For Mach 7.6 conditions, only Injection Distribution IR4 was experimented. With the initial combustor geometry, a significant discrepancy was observed between tests and computations. This was due to a deformation of the combustor during the tests, due to the great thermal stresses endured by the mock-up under these conditions. A consequence of this deformation was, in particular, a reduction of the cross-section at the end of the first part of the combustor. Taking into account the deformation of the combustor in the computations led to a better agreement with the experimental results, as seen in Figure 42 for ER=1. Due to the deformation, combustion is not fully supersonic: the flow is choked at the end of the first part of the combustor. Fully supersonic combustion was obtained only for ER<0.8.

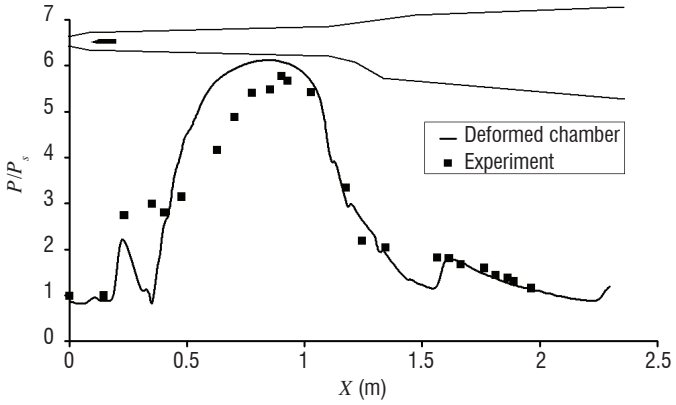

Figure 42 - Mach 7.6 - ER=1 - IR4 - Computed and experimental pressure distribution

The JAPHAR test campaign and the associated 3D computations demonstrated the possibility of operating a fixed geometry dual-mode ramjet at high equivalence ratio from Mach 4 to 8. The various combustion regimes that were predicted – subsonic, transonic and supersonic – were experimentally observed. Furthermore, it was shown that the shock and thermal throat positions could be controlled by adjusting the injection distribution. A very good agreement between computation and experimental results was obtained. More detailed information can be found in [59], [60], [61].

Test and Nose-to-Tail simulation of the SSFE scramjet

As the flight Mach number increases to supersonic and hypersonic values, it becomes necessary to carefully integrate the propulsion system on the airframe, in order to maximize inlet performance while limiting engine mass and drag. A typical hypersonic vehicle layout can be seen in Figure 43: much of the compression of the engine incoming air flow is produced by the vehicle fore-body; conversely, the after-body is used for the expansion process.

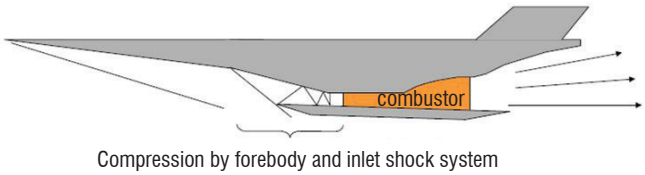

Figure 43 - Typical scramjet powered hypersonic vehicle layout

Therefore, in order to assess engine performance, it appears crucial to test it along with the entire vehicle, or at least with its entire flow path (i.e., the bottom of the fore and after-body). From an experimental point of view, free-jet facilities are thus required. These facilities must provide high total pressure and total enthalpy to simulate hypersonic flight Mach numbers.

From a numerical point of view, simulations must be conducted on the entire vehicle, including the combustion process in the engine. Various approaches can be considered for these 'Nose-to-Tail' (NtT) computations. It is possible to take advantage of the hyperbolic nature of the steady supersonic Navier-Stokes equations [62]. Then, computation can be performed 'by blocks', with each block being fed by the upstream block and feeding the downstream one. In addition, Parabolized Navier-Stokes can be used for the airframe. In the combustor, where large zones of subsonic flow can occur, various approaches can be used, from the zero-dimensional study to the tree-dimensional unsteady Navier-Stokes computations (RANS or LES). However, with increasing computational capabilities, 'integrated' NtT simulations (only one block for the whole computation) can now be considered.

We compare here free-jet tests of a hypersonic vehicle small-scale model in the ONERA F4 hyper-enthalpy arc-heated wind-tunnel, with NtT simulations performed with the ONERA code CEDRE.

The model tested here is a small-scale wave-rider (see Figure 44) designed by ESTEC [63][64][65] and manufactured by the DLR within the framework of the LAPCAT II European program (Long-term Advanced Propulsion Concepts and Technologies, funded by the European Commission as part of the 7th Framework Program and involving 16 European research labs and industries). This model has also been tested in the DLR high enthalpy shock tunnel [66] (HEG). The original vehicle is 94m long, 41m wide and weighs 400 tons at take-off. The 1.44 m long small-scale version, designed for the wind tunnel experiments, is also known as the SSFE (Small Scale Flight Experiment) model. Figure 45 shows the SSFE model installed

in the F4 test section. For obstruction reasons, and because only the internal flow path is being analyzed, the wings have not been machined. Adequate air/fuel mixing is obtained using three injection struts. Two struts are placed close to the combustor inlet at x=450 mm and another is placed farther downstream in the symmetry plane, at x=600 mm. The model is equipped with 40 Kulite pressure sensors.

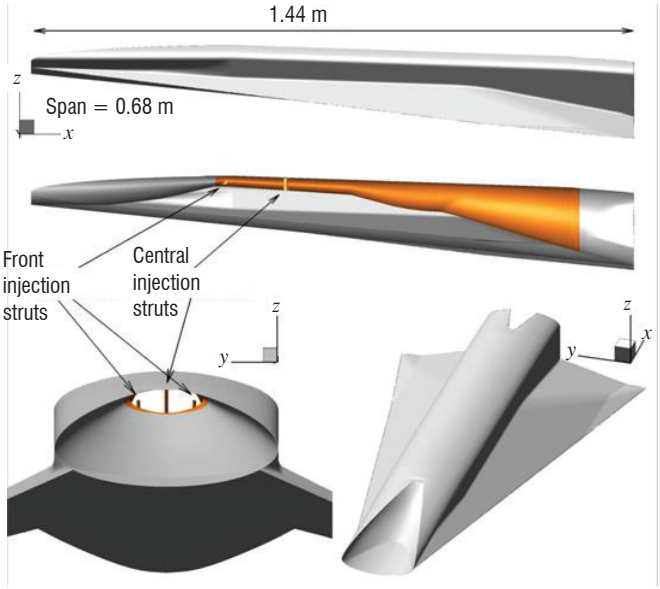

Figure 44 - CAD views of the ESTEC wave-rider model

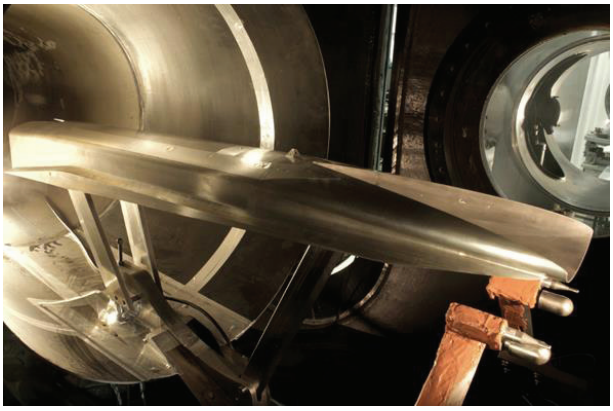

Figure 45 - View of the SSFE model installed in the F4 test section

Combustor pressure profiles for two runs (R1334 & R1343) at Mach 8 are presented in Figure 46 and Figure 47. Run R1334 is fuel-off, whereas Run R1343 is fuel-on with an equivalence ratio equal to 1. Pitot pressures in the test section and total enthalpy are given in the figures. CFD simulations are conducted considering:

1. a fully turbulent boundary-layer (Menter's SST turbulence model).
2. a fully laminar boundary-layer.
3. a transitional boundary-layer (the transition location is set 'artificially' at combustor inlet).

Fuel-off simulations (Figure 46) show that taking into account the transition on the fore-body of the vehicle is of prime importance when computing the flow in the engine. This highlights the strong dependence of the engine flow on the fore-body flow for hypersonic vehicles and the interest of free-jet testing and NtT simulation.

Fuel-on results are shown in Figure 47 for the transitional case. A good agreement is obtained in the first part of the combustor (x<700 mm), then the simulation under-predicts pressure levels. Several reasons can be considered to explain this discrepancy, but the most acceptable one is the air vitiation due to the electric arc that is used to generate hyper-enthalpy conditions in the arc chamber of the wind-tunnel.

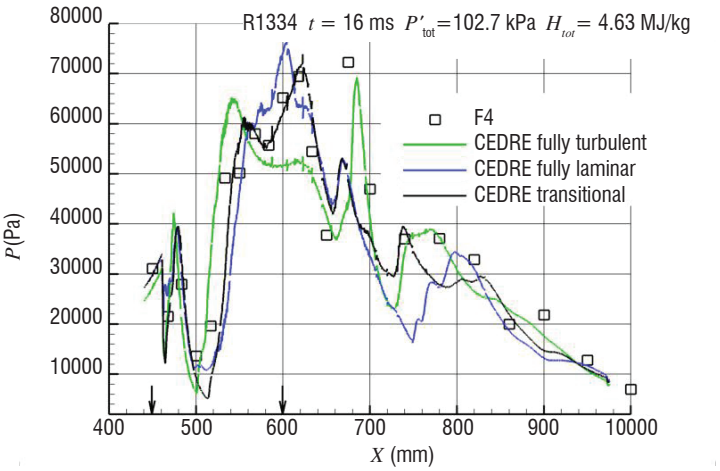

Figure 46 - R1334. Test / CFD comparison of pressure profiles for the three boundary layer transition modeling (the arrows show the injection locations)

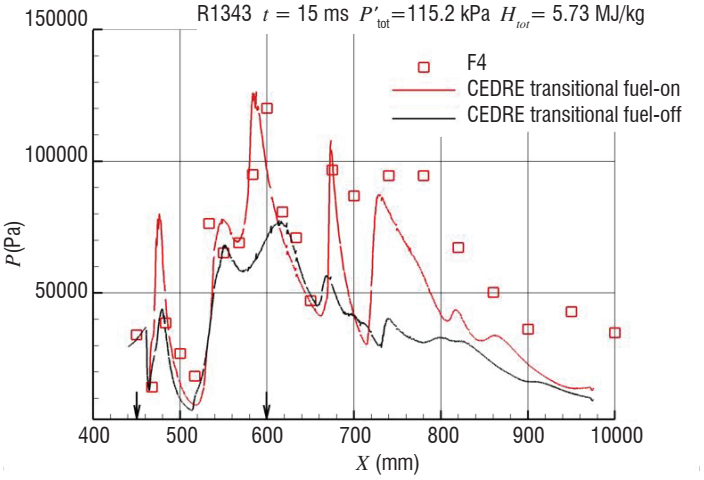

Figure 47 - R1343. Test / CFD comparison of pressure profiles (the arrows show the injection locations)

Conclusion

After a ten year period between 1962 and 1972, studies on supersonic combustion ramjets were stopped at ONERA for twenty years, mainly due to the difficulty in assessing the propulsive balance of an airbreathing hypersonic vehicle with sufficient accuracy. For this reason, the decision was made to concentrate efforts on rocket engines for high-speed propulsion. Since the renewal of scramjet activities in 1992, successive important programs have allowed a significant research activity to be maintained at ONERA and MBDA, its industrial partner, on this topic. The physics of supersonic combustion is now well understood, in particular the various and complex interactions between aerodynamics and heat release. Thanks to the development of both codes and supercomputers, CFD predictions are today reasonably reliable, so the design process of an airbreathing hypersonic vehicle has been mastered. However, the capacity to accurately predict the propulsive balance of such a vehicle from computations and ground tests is still perfectible, due to the great sensitivity of the propulsive balance to any small error in the outcoming impulse: progress on this aspect remains a key issue for the development of airbreathing hypersonic vehicles in the future ■

Acknowledgements

ONERA wishes to thank all of its partners in research programs on supersonic combustion, in particular MBDA, DLR, JAXA, ESA and ITLR. Special thanks to A. Mura (ENSMA) for fruitful discussions and for his contribution to the modeling activities.

References

[1] A. MESTRE, L. VIAUD - *Combustion supersonique dans un canal cylindrique.* Supersonic flow chemical processes and radiative transfer, D.B. Olfe, V. Zakkay, Pergamon Press, 1964

[2] R. MARGUET, C. HUET - *Recherche d'une solution optimale de statoréacteur à géométrie fixe, de Mach 3 à 7, avec combustion subsonique puis supersonique.* T.P. ONERA n°656, 1968

[3] F. HIRSINGER - *Optimisation des performances d'un statoréacteur supersonique - Etude théorique et expérimentale.* ISABE, Marseille, 1972, T.P. ONERA n° 1106

[4] O. LEUCHTER - *Etude des évolutions chimiques dans une couche de mélange hydrogène-air.* T.P. ONERA n° 981 , 1971

[5] O. LEUCHTER - *Problèmes de mélange et de combustion supersonique d'hydrogène dans un statoréacteur hypersonique.* T.P. ONERA n° 973, 1971

[6] F. FALEMPIN, D. SCHERRER, G. LARUELLE, P. ROSTAND, G. FRATACCI, J.L. SCHULTZ - *French Hypersonic Propulsion Program PREPHA - Results, Lessons and Perspectives.* 8th International Space Planes and Hypersonic Systems and Technologies Conference, AIAA-98-1565, April 27-30, 1998, Norfolk

[7] P. NOVELLI, W. KOSCHEL - *JAPHAR – A Joint ONERA-DLR Research Project on High Speed Airbreathing Propulsion.* ISABE paper 99-7091, 14th Symposium ISABE, Florence (Italy), September 05-10, 1999

[8] P. NOVELLI, W. KOSCHEL - *Progress of the JAPHAR Cooperation Between ONERA and DLR on Hypersonic Airbreathing Propulsion.* 10th International Space Planes and Hypersonic Systems and Technologies Conference, Kyoto (Japan), AIAA 2001-1870, April 24-27, 2001

[9] T. SUNAMI, P. MAGRE, A. BRESSON, F. GRISCH, M. ORAIN, M. KODERA - *Experimental Study of Strut Injectors in a Supersonic Combustor Using OH-*PLIF. 13th International Space Planes and Hypersonic Systems and Technologies Conference, May 16-20, 2005, Capua, Italy

[10] J. STEELANT - *Sustained Hypersonic Flight in Europe: First Technology Achievements within LAPCAT II.* 17th AIAA International Space Planes and Hypersonic Systems and Technologies Conference, San Francisco (CA), 2011, AIAA 2011–2243

[11] J. STEELANT, R. VARVILL, S. DEFOORT, K. HANNEMANN, M. MARINI - *Achievements Obtained for Sustained Hypersonic Flight within the LAPCAT II Project,* 20th International Space Planes and Hypersonic Systems and Technologies Conference, AIAA-2015-3677, Glasgow, UK, 5-8 July 2015

[12] A. BRESSON - *OH/Acetone* PLIF *and CARS Thermometry in a Supersonic Reactive Layer.* 10th International Space Planes and Hypersonic Systems and Technologies Conference, Kyoto (Japan), April 24-27, 2001

[13] P. MAGRE, P. BOUCHARDY - *Nitrogen and Hydrogen Coherent Anti-Stokes Raman Scattering Thermometry in a Supersonic Reactive Mixing Layer.* Proceedings of the Combustion Institute, Volume 28, Issue 1, 2000, pp. 697-703

[14] D. FOURNET, P. MAGRE, G. COLLIN - *Mesure de Profils de Vitesse par Vélocimétrie Laser dans un Ecoulement Supersonique en Combustion.* 6é Congrès Francophone de Vélocimétrie Laser, Saint-Louis, France, 22-25 September 1998

[15] H. WEISGERBER, R. MARTUNOZZI, U. BRUMMUND, P. MAGRE - *PIV Measurements in a Mach 2 Hydrogen-Air Supersonic Combustion.* AIAA-2001-1757. 10th International Space Planes and Hypersonic Systems and Technologies Conference, Kyoto (Japan), April 24-27, 2001

[16] E. GEORGE, P. MAGRE, V. SABEL'NIKOV - *Self-Ignition of Hydrogen-Hydrocarbons Mixtures in a Hot Supersonic Confined Coflow of Air.* 13th AIAA International Space Planes and Hypersonic Systems and Technologies Conference, 2005

[17] D. GAFFIÉ, U. WEPLER, P. MAGRE, W. KOSCHEL, P. NOVELLI - *Numerical Investigation of Supersonic Reacting Hydrogen Jets in a Hot Air Coflow.* 10th AIAA International Space Planes and Hypersonic Systems and Technologies Conference, 2001

[18] D. DAVIDENKO, I. GÖKALP, E. DUFOUR, D. GAFFIÉ - *Kinetic Mechanism Validation and Numerical Simulation of Supersonic Combustion of Methane-hydrogen Fuel.* 11th AIAA International Space Planes and Hypersonic Systems and Technologies Conference, 2002

[19] V. QUINTILLA, P. MAGRE, D. SCHERRER, P. DESTORS, E. DUFOUR - *Experimental and Numerical Investigation of Supersonic Reacting Hydrogen/Methane Jets in hot Air Coflows.* 13th AIAA International Space Planes and Hypersonic Systems and Technologies Conference, May 16-20, 2005, Capua, Italy

[20] L. VULIS - *Thermal Regimes of Combustion*, McGraw-Hill, New York, 1961

[21] B. MAGNUSSEN - *On the Structure of Turbulence and a Generalised Eddy Dissipation Concept for Chemical Reactions in Turbulent Flow,* 19th AIAA Aerospace Sciences Meeting, 1981

[22] B. MAGNUSSEN - *The Eddy Dissipation Concept.* ECCOMAS Thematic Conference on Computational Combustion, 2005

[23] I. ERTESVAG, B. MAGNUSSEN - *The Eddy Dissipation Turbulent Energy Cascade Model.* Combust. Sci. Technol. 159 (1) (2000) 213–235

[24] M. BERGLUND, E. FEDINA, C. FUREBY, J. TEGNER, V.A. SABEL'NIKOV - *Finite Rate Chemistry Large Eddy Simulation of Self-Ignition in Supersonic Combustion Ramjet.* AIAA Journal, Vol. 48, No 3, March 2010 , pp. 540–550

[25] Y. MOULE, V.A. SABEL'NIKOV, M. SMART, A. MURA - *Computational Fluid Dynamics Investigation of a Mach 12 Scramjet Engine.* J. Propul. Power 30, 2014, pp. 461–473

[26] A. LINÁN - ACTA ASTRON. 1, 1974, pp. 1007–1039

[27] O. JARRETT, A. CUTLER, R. ANTCLIFF, T. CHITSOMBOON, C. DANCEY, J. WANG - *Measurements of Temperature, Density, and Velocity in Supersonic Reacting Flow for CFD Code Validation.* 25th JANNAF Combustion Meeting, vol. 1, 1988, pp. 357–374

[28] T. CHENG, J. WEHRMEYER, R. PITZ, O. JARRETT, G. NORTHAM - *Finite-Rate Chemistry Effects in a Mach 2 Reacting Flow.* 27th AIAA Joint Propulsion Conference, 1991

[29] T. CHENG, J. WEHRMEYER, R. PITZ, O. JARRETT, G. NORTHAM - *Raman Measurement of Mixing and Finite-Rate Chemistry in a Supersonic Hydrogen-Air Diffusion Flame.* Combustion and Flame, Vol 99, Issue 1, 1994, pp. 157-173

[30] C. DANCEY - *The Turbulent Flow Field Downstream of an Axisymmetric Mach 2 Supersonic Burner: LDA Measurements.* 32nd AIAA Joint Propulsion Conference, 1996

[31] C. JACHIMOWSKI - *An Analysis of Combustion Studies in Shock Expansion Tunnels and Reflected Shock Tunnels.* Tech. Rep., NASA, 1992

[32] A. REFLOCH, B. COURBET, A. MURRONE, P. VILLEDIEU, C. LAURENT, P. GILBANK, J. TROYES,L. TESSÉ, G. CHAINERAY, J. DARGAUD, E. QUÉMERAIS, F. VUILLOT - *CEDRE Software*. Aerospace Lab Journal 2, 2011

[33] D. SCHERRER, F. CHEDEVERGNE, P. GRENARD, J. TROYES, A. MURRONE, E. MONTREUIL, A. CHAZOTTES, F. VUILLOT, N. LUPOGLAZOFF, M. HUET, B. SAINTE-ROSE, P. THORIGNY, N.BERTIER, J.-M. LAMET, T. LE PICHON, E. RADENAC, A. NICOLE, L. MATUSZEWSKI, M.ERRERA - *Recent CEDRE Applications.* Aerospace Lab Journal 2, 2011

[34] E. TORO, M. SPRUCE, W. SPEARES - *Restoration of the Contact Surface in the HLL-Riemann Solver*. Shock Waves 4 , 1994, pp. 25-34

[35] P. GERLINGER, K. NOLD, M. AIGNER - *Influence of Reaction Mechanisms, Grid-Spacing, and Inflow Conditions on the Numerical Simulation of Lifted Supersonic Flames*. Int. J. Numer. Methods Fluids 62 , Issue 12, 2010, pp. 1357-1380

[36] S. KARL - *Numerical Investigation of a Generic Scramjet Configuration*. Ph.D. thesis, The University of Dresden, 2011

[37] P. BOIVIN, A. DAUPTAIN, C. JIMÉNEZ, B. CUENOT - *Simulation of a Supersonic Hydrogen-Air Auto-Ignition Stabilized Flame Using Reduced Chemistry*. Combustion and Flame, Vol 159, Issue 4, 2012, pp. 1779–1790

[38] Y. MOULE, V. SABEL'NIKOV, A. MURA - *Highly Resolved Numerical Simulation of Combustion in Supersonic Hydrogen-Air Coflowing Jets.* Combustion and Flame 161 (2014), pp. 2647-2668

[39] Y. MOULE - *Modélisation et simulation de la combustion dans les écoulements rapides*. Applications aux Superstatoréacteurs, ENSMA PhD Thesis, 2013

[40] A. BEN-YAKAR, M. MUNGAL, R. HANSON - *Time Evolution and Mixing Characteristics of Hydrogen and Ethylene Transverse Jets in Supersonic Crossbows*. Physics of Fluids 18, 026101 (2006)

[41] V. VITI, R. NEEL, J. SCHETZ - *Detailed Flow Physics of the Supersonic Jet Interaction Flow Field*. Physics of Fluids 21 (2009)

[42] S. KAWAI, S. LELE - *Large-Eddy Simulation of Jet Mixing in Supersonic Crossflows*. AIAA Journal 48, 2063-2083 (2010)

[43] M. GAMBA, V. MILLER, M. GODFREY MUNGAL - *The Reacting Transverse Jet in Supersonic Crossow: Physics and Properties.* AIAA paper 2014-3107, AIAA Aviation / 19th AIAA International Space Planes and Hypersonic Systems and Technologies Conference (Atlanta, Georgia, 16-20 June, 2014)

[44] D. SCHERRER - *Optimisation de l'injection d'hydrogène dans un écoulement d'air supersonique*. 1er Colloque du Programme de Recherches Concertées Combustion dans les Superstatoréacteurs, CNRS, Paris, 21-22 October 1991

[45] D. SCHERRER, O. DESSORNES, N. MONTMAYEUR, O. FERRANDON - *Injection Studies in the French Hypersonic Technology Program*. AIAA-95-6096, 6th International Space Planes and Hypersonic Systems and Technologies Conference, April 3-7, 1995, Chattanooga

[46] O. DESSORNES, C. JOURDREN - *Mixing Enhancement Techniques in a Scramjet*. AIAA-98-1517. 8th International Space Planes and Hypersonic Systems and Technologies Conference, April 27-30, 1998, Norfolk

[47] J. SWITHENBANK, N.A. CHIGIER - *Vortex Mixing for Supersonic Combustion*. Proceedings of the 12th Symposium (International) on Combustion, 1968, pp. 1153-1162

[48] L.A. POVINELLI, F.P. POVINELLI, M. HERSCH - *A study of Helium Penetration and Spreading in a Mach 2 Airstream Using a Delta Wing Injector*. NASA TN D-5322, 1969

[49] G.B. NORTHAM, I. GREENBERG, C.S. BYINGTON - *Evaluation of Parallel Injector Configurations for Supersonic Combustion*. AIAA-89-2525, 1989

[50] E.J. GUTMARK, K.C. SCHADOW,, K.H. YU - *Mixing Enhancement in Supersonic Free Shear Flows*. Annual Review of Fluid Mechanics, Vol. 27, 1995, pp. 375-417

[51] M. NISHIOKA, T. SUNAMI - *Some Thoughts and Experiments on the Supersonic Mixing Enhancement*. Journal of fluid Mechanics of Japan, Vol. 14, pp. 377-389, 1995 (in Japanese)

[52] T. SUNAMI, M.N. WENDT, M. NISHIOKA - *Supersonic Mixing and Combustion Control Using Streamwise Vortices.* AIAA-98-3271, 1998

[53] T. SUNAMI, A. MURAKAMI, K. KUDO, M. KODERA, M. NISHIOKA - *Mixing and Combustion Control Strategies for Efficient Scramjet Operation in Wide Range of Flight Mach Numbers*. AIAA-2002-5116, 11th International Space Planes and Hypersonic Systems and Technologies Conference, 1992, Orléans

[54] T. SUNAMI, P. MAGRE, A. BRESSON, F. GRISCH, M. ORAIN, M. KODERA - *Experimental Study of Strut Injectors in a Supersonic Combustor Using OH*-PLIF. 13th International Space Planes and Hypersonic Systems and Technologies Conference, May 16-20, 2005, Capua, Italy

[55] C. FUREBY, K. NORDIN-BATES, K. PETTERSON, A. BRESSON, V. SABELNIKOV - *A Computational Study of Supersonic Combustion in Strut Injector and Hypermixer Flow Fields*. Proceedings of the Combustion Institute 35 (2), 2015, pp. 2127-2135

[56] A. VINCENT-RANDONNIER, Y. MOULE, M. FERRIER - *Combustion of Hydrogen in Hot Air Flows within LAPCAT–II Dual Mode Ramjet Combustor at Onera-LAERTE Facility – Experimental and Numerical Investigation*. 19th AIAA International Space Planes and Hypersonic Systems and Technologies Conference, Atlanta (GA), 2014, AIAA 2014–2932

[57] S. DEFOORT, M. FERRIER, L. SERRE, D. SCHERRER, C. PARIDAENS, P. HENDRICK, A. INGENITO, C. BRUNO - L*APCAT-II: Conceptual Design of a Mach 8 TBCC Civil Aircraft, Enforced by Full Navier-Stokes 3D Nose-to-Tail Computation.* 17th AIAA International Space Planes and Hypersonic Systems and Technologies Conference, San Francisco (CA), 2011, AIAA 2011–2317

[58] A. BEN-YAKAR, R. HANSON - *Experimental Investigation of Flame-Holding Capability of Hydrogen Transverse Jet in Supersonic Cross-Flow.* 36th Int. Symp. on Combustion, 27 (2), 1998, 2173-2180

[59] O. DESSORNES, D. SCHERRER, P. NOVELLI - *Testing and Weighing of the Japhar Dual Mode Ramjet Engine*. ISABE paper 2001-1135, Bengalore (India)

[60] O. DESSORNES, D. SCHERRER - *Weighing of the JAPHAR Dual Mode Ramjet Engine*. AIAA paper 2002-5187, Orléans (France), 2002

[61] O. DESSORNES, D. SCHERRER - *Tests of the JAPHAR Dual Mode Ramjet Engine*. Aerospace Science and Technology, 2005, volume 9, issue 3, pages 211-221

[62] C.E.JR. COCKRELL, W.C. ENGELUND, R.D. BITTNER, T.N. JENTINK, A.D. DILLEY, A. FRENDI - I*ntegrated Aeropropulsive Computational Fluid Dynamics Methodology for the Hyper-X Flight Experiment.* Journal of Spacecraft and Rockets 38-6 (2001)

[63] T. LANGENER, J. STEELANT, S. KARL, K. HANNEMANN - *Design and Optimization of a Small Scale Mach=8 Scramjet Propulsion System*. Space Propulsion 2012. SP2012-2394071, May 2012, Bordeaux, France

[64] T. LANGENER, J. STEELANT, S. KARL, K. HANNEMANN - *Layout and Design Verification of a Small Scale Scramjet Combustion Chamber.* 21st International Symposium on Air breathing Engine. ISABE-2013-1655, September 9-13 2013, Busan, Korea

[65] T. LANGENER, J. STEELANT, S. KARL, K. HANNEMANN - *Numerical Validation of a Free-Flying Scramjet Powered Vehicle at Realistic Wind Tunnel Conditions.* Space Propulsion 2014. SP2014-2971766, May 19-22 2014, Cologne, Germany

[66] K. HANNEMANN, J. SCHRAMM, S. LAURENCE, S. KARL - *Experimental and Numerical Analysis of the small Scale LAPCAT II Scramjet Flow Path in High Enthalpy Shock Tunnel Conditions.* Space Propulsion 2014. SP2014-2969350, May 19-22 2014, Cologne, Germany

AUTHORS

Dominique Scherrer graduated from « Ecole Centrale de Paris » in 1979. He joined ONERA in the Energetics Direction in 1981. His main research topics concerned droplet combustion modeling, combined cycle propulsion, scramjet design and CFD. He has been the CEDRE project manager between 1996 and 2002. He is deputy director of the Fundamental and Applied Energetics Department since 1997.

Olivier Dessornes graduated from the French engineering school ESTACA in 1990. He joined ONERA in 1990 where he is a research engineer working in the Fundamental and Applied Energetics Department (DEFA). He is mostly involved in experimental activities. His current fields of interest are scramjet propulsion, energy micro sources and hybrid propulsion.

Marc Ferrier graduated from HEI (Lille) in 2002 and received his Ph.D. Degree in Fluid Dynamics in 2008 for his work on boundary layer transition in supersonic flow. He is now a research engineer at ONERA, where he works on supersonic combustion.

Axel Vincent-Randonnier graduated from Université Pierre et Marie Curie where he obtained MSc and PhD degrees in Energetics and Process Engineering in 2002. He joined ONERA in 2004 for post-doctoral activities on plasma assisted combustion. Since 2006, he has been in charge of LAERTE subsonic and supersonic combustion facilities at ONERA – Palaiseau Center. Since 2012, he has been in charge of the MICADO project aimed at developing a new test rig dedicated to the study of high-pressure air-breathing combustion with optical diagnostics.

Yann Moule graduated from ENSMA (Poitiers) in 2007 and received his Ph.D. Degree in Energetics in 2012. His research work at Onera focused on combustion in supersonic flows and scramjet engines. He joined MBDA France in 2014, where he is working as a propulsion engineer.

Vladimir Sabelnikov gratuated (1971) from Moscow Institute of Physics and Technology (MIPT), Dolgoprudny, Russia, Ph.D. (1974), and Doctor of Science (1984) degrees from MIPT also. In 1974, he joined the Central Aerohydrodynamics Institute (TsAGI, Moscow, Russia), where he was Leading Scientist until 2000. Since 2000, he is a Leading Scientist in Energetic department of ONERA. His current research interests include the study of combustion instabilities in gas turbines, supersonic combustion in ducts, scramjets, combustion in microcombustors, the plasma control of combustion, the development of Eulerian Monte Carlo method to solve the transported PDF equation in turbulent combustion, and the development of new PaSR and EPaSR models of turbulent combustion.

Office National d'Études et de Recherches Aérospatiales
Chemin de la Hunière et des Joncherettes – BP 80100
91123 PALAISEAU Cedex
Tél. : +33 1 80 38 60 60 - Fax : +33 1 80 38 65 10
http://www.onera.fr